J. theor. Biol. (1993) **164**, 477–506

Can Surface Adhesion Drive Cell Rearrangement? Part II: A Geometrical Model

FRANÇOIS GRANER† AND YASUJI SAWADA

Research Institute for Electrical Communications, Tohoku University, 2-1-1 Katahira, Sendai 980, *Japan*

(*Received on* 18 *August* 1992, *Accepted in revised form on* 26 *March* 1993)

We present a new flexible, geometrical and dynamical model for cell rearrangement. It includes free boundaries between the cells and the external medium, to account naturally for surface tension effects. The forces deriving from intercellular adhesion and membrane elasticity act on points representing polygonal cells, according to an extended Dirichlet construction. The model simulates the aggregation and rounding of an homogeneous cell collection and short-distance cell movements.

We then examine the behaviors of a mixture of two cell types: aggregate engulfment, cell dispersal, total and partial cell-sorting, and more exotic patterns, such as "position reversal" and the checkerboard. Including free boundaries causes long-distance cell movements, suggesting that cell surface adhesion can drive passive biological cells.

1. Introduction

In a wide range of vertebrates and invertebrates, cells can move and rearrange, for example during embryogenesis, healing and *in vitro* reaggregation. The mechanism of cell mobility is still debated in developmental biology (for a review, see Keller, 1987; Fristrom, 1988). Movement requires both a driving force and a guiding mechanism. Surface adhesion is known to guide cells in migration on substrates (Carter, 1967), cancer metastasis (Jouanneau *et al.*, 1991; Takeichi, 1991), the migration of the optic nerve axon (Fraser, 1985), and cell-sorting (see Armstrong, 1989 for a review). We suggest that cell–cell surface adhesion can be a driving force as well.

We have shown elsewhere (Graner, 1993) how cell–cell adhesion can drive cells lacking autonomous active motility. We can attribute a potential energy to a cellular pattern if adhesion energy is proportional to the contact area between two cells. The local energy gradient drives cells, as long as microscopic thermal fluctuations allow adhesive links to break and re-establish. The adhesive driving force arises from inhomogeneities, for example from boundaries with other cell types, the culture medium, the extracellular matrix or the substrate. Cells can deterministically change shape and position over distances comparable to the average cell radius R, without overcoming an energy barrier; thus, they need neither to have intrinsic motility, nor to randomly explore next nearest neighbor cells. Moreover, a collection of two

† Present address: Laboratoire de Physique Statistique, Ecole Normale Supérieure, 24 rue Lhomond, 75005 Paris, France.

0022–5193/93/020477+30 $08.00/0

TABLE 1
Some models of biological cells, which include both cell geometry and forces

Source	Honda (1978, 1983)	Honda *et al.* (1980, 1983, 1986)	Odell *et al.* (1981)	Childress & Percuss (1981)	Sulsky *et al.* (1984)	Weliky & Oster (1990)	Prunsinkiewicz & Lindenmayer (1990)	Present paper
Model name	Cell-aggregate	Boundary shortening	Purse-string	Stress relaxation	Dirichlet dynamics	Contraction protrusion	Map L-system	Free cells
Phenomena	Division and loss of cells	Healing, checkerboard	Gastrulation	Rounding Bending	Cell-sorting	Epiboly	Plant growth	Cell rearrangement
Geometry of cells	Dirichlet	Polygons	Symmetric polyedrons	Rectangles	Dirichlet	Polygons	Free polygons	Free Dirichlet
Gaps between cells	—	—	—	—	—	—	—	Yes
Dynamics of:	Center	Membrane	Membrane	Vertex	Center	Vertex	Vertex	Center
Boundary conditions	—	Fix, periodic	Free	Free	Periodic	Forced movement	Free	Free
Cell displacement	Local	—	—	Local	Local	Forced long-distance	—	Long-distance
Number of cell types	1	1, 2	1	1	2	1	1	1 or 2
Neighbor exchange	Yes	Yes	—	—	Yes	Yes	Yes	Yes

randomly mixed cell types can sort to re-establish homogeneous tissues. Gustafson & Wolpert (1963) have compared adhesion molecules to the teeth of a zipper which hold together two surfaces, but no "zipper fastener" other than nanometer-range thermal fluctuation is needed to close the zipper and bring cell membranes into contact.

In this paper we simulate surface-energy driven cellular patterns. No single model is best (for review, see Glazier *et al.*, 1993, in press). Early models of point-like cells rearranging on a lattice (Goel & Leith, 1970; Goel *et al.*, 1970; Leith & Goel, 1971; Gordon *et al.*, 1972; Antonelli *et al.*, 1973) turned insufficient (Steinberg, 1975). Later improvements take into account the geometrical/topological characteristics of the cellular pattern (Rogers & Sampson, 1977; Goel & Rogers, 1978; Rogers & Goel, 1978; Matela & Fletterick, 1979, 1980), forces between cells (Greenspan, 1981), or both (Table 1). But up to now, none had been able to describe consistently homogeneous and heterogeneous, two- (2D) and three-dimensional (3D), loose and compact aggregates. Section 2 presents a flexible model which naturally treats cell free boundaries and intercellular gaps in long-distance cell rearrangement. It can also describe short-range rearrangement, membrane elasticity, cell compressibility and internal pressure. It treats different types of force, particularly cell adhesion and differential adhesion, and can include gravity, centrifugation, and long-range cell interaction, for example, chemotaxis. Section 3 uses this model and examines if assuming that the adhesion energy is proportional to the cell–cell contact area yields a good description of biological cell rearrangement. Section 4 discusses the biological relevance of the simulations.

2. How Can We Model Cell Movement?

A complete description of an aggregate needs an infinity of position parameters and is not possible in a model. What parameters are necessary, and which negligible, in a geometrical model? Cell position and shape must vary smoothly to account for the continuous decrease or increase of contact areas. However, neighbor exchange is a topological singularity via a transient five-cell vertex (four cells in two dimensions, Fig. 1). Any model which does not describe such geometrical features misrepresents

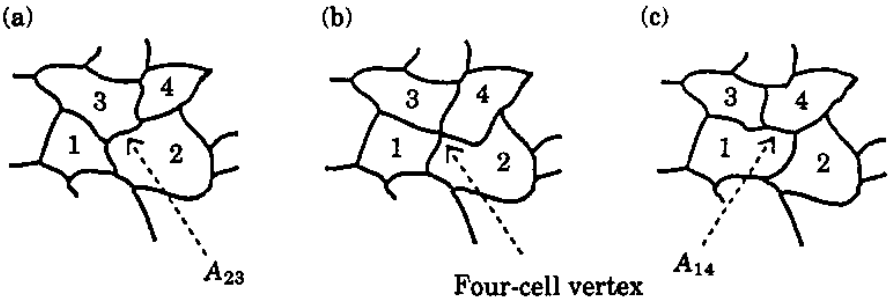

FIG. 1. Sketch of neighbor exchange in two dimensions (redrawn from Graner, 1993). (a) Cells 2 and 3 are separating, 1 and 4 approach. The membrane A_{23} shortens, the vertices 1.2.3 and 2.3.4 approach. (b) By continuity, the vertices 1.2.3 and 2.3.4 fuse to form a transient four-cell vertex; the membrane A_{23} disappears. (c) The cells still move continuously: 2 and 3 separate, 1 and 4 touch. A new membrane A_{14} and two new vertices 1.2.4 and 1.3.4 appear, replacing A_{23}, 1.2.3 and 2.3.4.

the evolution. Free Dirichlet domains are a simple method that realistically describes, with a few parameters, an evolution limited by the mobility of the centers where vertex positions relax quickly.

2.1. ORDINARY DIRICHLET DOMAINS

A Dirichlet domain is labeled by a center and is defined as the subset of the space which is closer to it than to all other centers. Equivalently, the boundary between two domains is the mediatrix plane between their centers. Domains are convex and cover the space. They are also known as Voronoi polygons, Wigner-Seitz cells, Meijering cells, Thiessen polygons, and are encountered in a variety of fields in physics and biology, when 2D or 3D patterns result from either growth initiated at centers, or competition between them (for reviews, see Weaire & Rivier, 1984; Frost, 1991). They also approximate well biological cell shapes, particularly for equilibrated epithelial cells (Honda, 1978), even though the Dirichlet center is neither the barycenter of the cell, nor its biological nucleus.

2.1.1. *Dirichlet domains: advantages*

A Dirichlet pattern of N cells is completely specified by the N positions $\vec{r}_i$ of the centers i. Each center is conserved during the evolution. It moves continuously in real space, not on a lattice. It experiences no singularities, even during neighbor rearrangement. The position of the centers automatically deletes and creates membranes and vertices. Cell areas and volumes can be calculated analytically as a simple function of the relative distances between centers, so that surface energies, compressions and elastic deformations can be computed using a minimal number of position parameters (Sulsky *et al.*, 1984). We can easily describe the effects of global forces and long distance movements, including global effects of differential adhesion, such as surface tensions, which arise from interactions between neighbors.

However, we do not neglect cell membrane topology (Matela & Fletterick, 1979, 1980). We can introduce forces acting on the membranes, such as pressure or adhesion. Geometrically, simulated shapes are flexible; hence, the agreement with biological local rearrangement, even in a non-equilibrated epithelium resulting from the addition or removal of a cell, by cell division or destruction (Honda, 1978, 1983).

2.1.2. *Dirichlet domains: cautions*

Arbitrary Dirichlet tilings cannot represent all biological cell aggregates. Care is needed. If the center positions are chosen at random, then the Dirichlet tiling has a broad distribution of cell volumes, and contact angles at vertices, with excessively irregular shapes. The cell volume distribution of model and biology must agree; if the cells to be represented have approximately the same size, then the centers must have initially a minimal separation (excluded volume) to produce an almost uniform density, internal contact angles at vertices close to 109·47° for identical cells (or 120° in two dimensions) and a realistic distribution of the number of faces or edges per cell (Glazier, 1989).

Honda (1983) started from a real cell distribution, so that the domain volumes and shapes were realistic. He studied the local relaxation far from the epithelium boundaries, but did not treat the boundaries, which are essential to understand adhesion-driven processes (Graner, 1993). In particular, surface tensions arising at free interfaces controls the demixion of intermingled cells of two different types. On the opposite, constrained boundary conditions distort demixion, either by pinning or increasing the mobility. Closed or periodic boundary conditions fix externally the average domains size; moreover, they regard a small portion of an aggregate as infinite.

Slow vertex rearrangement can be a limiting factor for evolution; for example, for an impermeable epithelium whose tight or septate junctions must adapt to new configurations (Keller & Trinkaus, 1987; Fristrom, 1988). If so, a vertex dynamics model is more appropriate. Such models allow flexible cell shapes and realistic representations, as in the simulations of *Fundulus* epiboly (Weliky & Oster, 1990). However, dynamics of non-conserved objects, such as membranes or vertices, need a set of creation and destruction rules, natural for neighbor exchange, but less easy to define at intercellular gaps or free boundaries (Weliky *et al.*, 1991).

2.2. THE MODEL

2.2.1. *Free Dirichlet domains*

We define "free Dirichlet domains" to include two features of biological cells: individual boundaries and characteristic size. As for ordinary Dirichlet domains, we denote each cell by a center. The cell is the subset of the space which is nearer to its center than to any other, but with the additional constraint that the distance from the center must be less than R [Fig. 2(a), 16].

FIG. 2. Free Dirichlet domains in 2D or 3D are labeled by their "centers" (dots). Each point of one domain is closer to its center than a distance R, than to any other center. A free membrane is a spherical cap of radius R, a contact surface is the mediatrix plane between two centers. (a) At each time-step the contact lengths are calculated as a function of the center positions. The surface energy is computed, along with its spatial derivatives (Appendix A). Segments indicate the force acting on each cell, i.e. the displacement during the next time step. All cells are then moved simultaneously and a new iteration starts. (b) Equilibrium state, after ≈ 1 min ($0{\cdot}055\tau_0$). An isolated cell does not move. The competition between surface adhesion and membrane elasticity determines the final contact lengths for two and three cells. *In this picture, as in Figs 5–15, dark (d) cells are more cohesive than light (l) cells, $e_{dd} < e_{ll}$. Here, surface energies are the same as in the cell-sorting case (Figs 10–12): $e_{dM} = e_{lM} = 0$; $e_{dd} = -12E_0$; $e_{dl} = -5E_0$; $e_{ll} = -2E_0$. Corresponding surface tensions are $\gamma_{dM} = 6E_0$, $\gamma_{dl} = 2E_0$, $\gamma_{lM} = E_0$. E_0 is a typical energy scale associated [eqn (8)] with a time scale τ_0 of the order 10^3 sec, which is used above and in the following captions. The number of time-steps has no physical significance since we use an adaptative time discretization procedure defined in Appendix C. Cell rigidity is determined to constrain the cell size without affecting position relaxation, see Appendix B.*

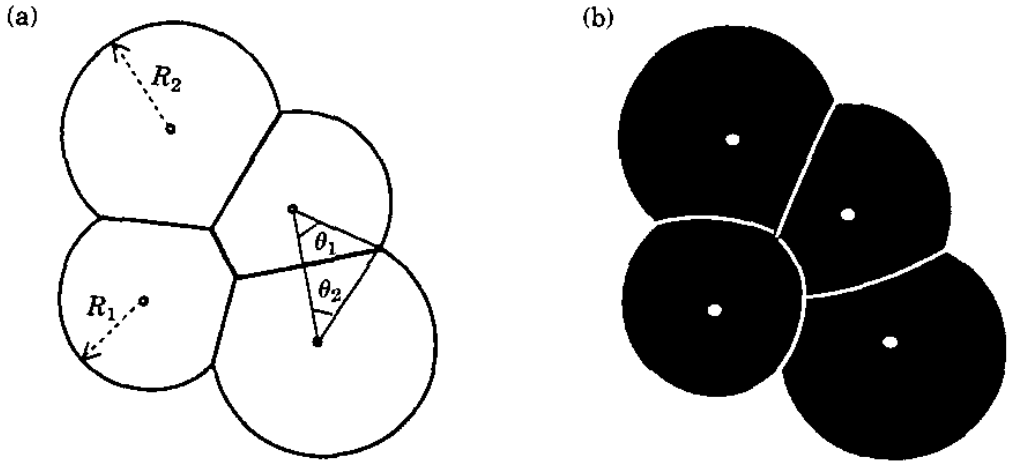

FIG. 3. Variants of Dirichlet domains. (a) Definitions of Dirichlet domains can be slightly altered for two cell types with different sizes R_1, R_2. Here, $R_1 \cdot \sin\theta_1 = R_2 \cdot \sin\theta_2$; and $R_1 \cdot \cos\theta_1 + R_2 \cdot \cos\theta_2 = r$, the distance between the two centers. These two conditions uniquely fix the positions of the membranes and ensure that three contiguous membranes actually meet, whatever the configuration. (b) If membrane shapes equilibrate more quickly than the cell internal pressure, they are spherical caps obeying Laplace's law.

If two centers are closer than $2R$, their mediatrix plane is the contact surface between their cells. But if two neighboring centers are further than $2R$, each cell has a free membrane, a spherical cap with radius R. R is a typical length scale, not the diameter of the domain, but an upper bound. An isolated domain is spherical, which is realistic for an isolated suspended cell. Each domain bound to a neighbor is convex and contained in a sphere of radius R; its volume and area are always smaller than $4\pi R^3/3$ and $4\pi R^2$. Equivalent domains in two dimensions are defined the same way. Such free domains can be defined with any boundary conditions, free or constrained. For fixed or periodic boundary conditions, if the average size allotted to each cell is much smaller than R, then no cell has any free membrane and the pattern is strictly equivalent to a normal Dirichlet tiling.

The essential feature of our model is this finite length scale, other details are not crucial. For instance, if the difference of hydrostatic/osmotic pressure between cells does not equilibrate by diffusion through the membrane more quickly than cell shapes do, then the membranes between cells can be described by spherical caps to include pressure differences [Fig. 3(b)]. Free membranes with constant R, and plane contact surfaces, occur if pressure differences among the cells equilibrate faster than membrane shapes. The model is also realistic for cells tightly packed under either extracellular or cytoskeletal interaction.

2.2.2. *Discussion of the representation*

Free Dirichlet domains experience no singularity, not only during neighbor exchange, but also when a center loses neighbors by drifting towards the edge of the cellular pattern. Instead of stretching and unrealistically elongating, the domain detaches from its neighbors and a portion of its membrane becomes free. If cell density is low and cells are not very adhesive, intercellular gaps can exist. The

representation is thus suitable even for loose aggregates or subconfluent monolayers (e.g. Steinberg & Garrod, 1975).

Numerically, computing Dirichlet tesselations is time-consuming but straightforward (Appendices A and C). Even with our modification, the areas of Dirichlet domains are still analytically defined as functions of the relative distances $r_{ij} = |\vec{r}_{ij}| = |\vec{r}_j - \vec{r}_i|$ between neighboring centers only. The set of the distances between centers whose domains share a vertex suffices to calculate not only geometrical quantities, such as the volumes and areas of the domains, but also their derivatives.

2.2.3. *Other examples of free Dirichlet domains*

Independent spherical cells, when aggregated and tightly compressed, deform into polyhedra which can be described by Dirichlet domains (Marvin, 1939; Matzke, 1939; Honda, 1983). Contact surfaces are plane, while intact surfaces keep the initial radius of the spheres.

Schulze & Wilbert (1989) have photographed a natural example of free Dirichlet domains in a film of crystallized isotactic polypropylene. Grains nucleate simultaneously and have the same growth velocity. When the circles impinge, the grain boundaries are the mediatrix of the nucleation sites, and grains are almost perfect two-dimensional-free Dirichlet domains. Gaps then progressively disappear as the crystallized fraction invades the whole film. Bénard & Dauzère (1913) filmed similar images of isolated cellular vortices in a Bénard free-surface convection experiment.

Finite size domains appear in territory competition between animals, a common example of Dirichlet tiling (Hasegawa & Tanemura, 1976). If the animals have a defense capacity with a finite range when their population is low, empty spaces appear. These available sites are repopulated by intercalation if the population increases.

Analogously, when French revolutionaries decided to design new "départements", it was proposed that every citizen should be able to ride by horse to his prefectural city, ideally the city nearest his home, in less than a day (Bredin, 1988), which constrained the departments to be contained with a rough 30–40 km radius circle, and fixed a lower bound on the number of domains necessary to cover the whole country.

2.2.4. *Interaction energy*

We wish to study the dynamics of a cellular pattern with a surface energy between a domain i and its neighbors j, e_{ij}, or the external medium, e_{iM}. The total adhesion energy (Graner, 1993),

$$E_{\text{adh}} = \sum_{\text{pair}(i,j)} S_{ij} e_{ij} + \sum_{i} S_{iM} e_{iM}, \tag{1}$$

associated to a given configuration of N cells, can be written as a function of the center positions (Appendix A):

$$E_{\text{adh}} = E_{\text{adh}}(\vec{r}_1, \ldots, \vec{r}_N) \tag{2a}$$

$$= \sum_{(i,j,k,l)} E_{\text{adh}}(\vec{r}_i, \vec{r}_j, \vec{r}_k, \vec{r}_l). \tag{2b}$$

In this summation $i = 1, \ldots, N$ and the quadruplet *ijkl* refers to domains sharing a vertex or a gap. As the energy of a quadruplet depends only on the relative distances between centers:

$$E_{\text{adh}}(\vec{r}_i\, \vec{r}_j, \vec{r}_k, \vec{r}_l) = E_{\text{adh}}(r_{ij}, r_{ik}, r_{il}, r_{jk}, r_{jl}, r_{kl}), \tag{3}$$

E_{adh} is a four-body potential interaction energy for the centers, each quadruplet independent of the others. In two dimensions, a triplet of domains shares a vertex and E_{adh} is a three-body interaction potential (Fig. 2 and Appendix A):

$$E_{\text{adh}}(2\text{D}) = \sum_{(i,j,k)} E_{\text{adh}}(r_{ij}, r_{jk}, r_{ki}). \tag{4}$$

Due to the negative adhesion surface energies, minimizing E_{adh} would result in a continuous increase of domain sizes. However, the bulk compressibility or the membrane elasticity provide a contribution, E_{stab}, to the total energy which constrains the volume, or area, of a biological cell near a given value, indirectly setting a lower bound on cell size (section 3.1 and Appendix B, Graner, 1993). We use E_{stab} to account for each cell's finite size, not for any specific "boundary shortening" as described by Honda (1983). Here, boundary shortening appears only as one aspect of decreasing E_{adh}.

2.2.5. *Force*

The total energy $E_{\text{total}}(\vec{r}_1, \ldots, \vec{r}_N)$ defines an energy landscape in the space of all possible domain configurations, labeled by the $3N$ co-ordinates $x_1, y_1, z_1, \ldots, z_N$. Each center i feels the local effect of the whole energy gradient, which acts on it as a force:

$$\vec{F}_i = -\vec{\nabla}_i E_{\text{total}}(\vec{r}_1, \ldots, \vec{r}_N) = -\frac{\partial E_{\text{total}}(\vec{r}_1, \ldots, \vec{r}_N)}{\partial \vec{r}_i}. \tag{5}$$

As E_{total} is a function of the relative positions $\vec{r}_{ij}$ only, we rewrite $\vec{F}_i$ as a sum over interactions with its neighbors j (Appendix A):

$$\vec{F}_i = \sum_j \frac{\partial E_{\text{total}}}{\partial r_{ij}} \frac{\vec{r}_{ij}}{r_{ij}}. \tag{6}$$

This force moves the center i to minimize the *total* configuration energy of the pattern along the steepest path of the energy landscape. If even one domain is out of equilibrium, for instance, because of adhesion inhomogeneities around it, it experiences a force, moves and acts on its neighbors. The whole pattern relaxes the initial local deformation coherently. Thus, the pattern can rearrange under the effect of surface tensions to diminish the energy of macroscopic heterotypic interfaces. Cells are interdependent, in the following sense.

In homogeneous identical domains, minimizing the energy involves minimizing the interface with the external medium. If it touches a substrate, an aggregate spreads or retracts depending on the wetting angle; in an homogeneous medium, it becomes spherical. If you add one cell at the surface of an already spherical aggregate, the

whole aggregate reorganizes to insert the new cell and become spherical again; this is the result of each non-equilibrated cell acting on its neighbors.

In a heterogeneous pattern, differential adhesivity results locally in either mixing or sorting of cell types according to their relative surface energies and may lead to a configuration with global energy minimum.

In both homogeneous and mixed cell patterns, surface tensions tend to reduce contact areas. They tend to smooth out the curvatures and mainly affect the highly curved interfaces.

All Newtonian conservation laws are satisfied since the forces derive from a symmetric, homogeneous and isotropic potential energy. Even if other factors contribute to the total energy, we can analytically derive its gradient with respect to the center positions as long as it is a function of geometrical quantities only. The force $\vec{F}_i$ is then a known function of the $\vec{r}_i$ and can also include gravity or centrifugation forces.

2.2.6. *Evolution equation*

During biological cell rearrangement, the cell inertia is negligible compared to viscous dissipation, so that evolution is a slow relaxation along the energy gradient; the way dissipation is modeled is then unimportant (Appendix D). We chose here a cellular description: each domain has a viscous drag proportional to its velocity, $\vec{F}_{\text{visc}} = -\mu_c \vec{v}$. The evolution equation is then deterministic (although we can incorporate other forces $\vec{F}_{\text{others}}$ not deriving from an energy, such as random fluctuations):

$$\vec{v}_i = \frac{\mathrm{d}\vec{r}_i}{\mathrm{d}t} = \frac{1}{\mu_c} \vec{F}_i. \tag{7}$$

3. Numerical Computations

3.1. METHODS

We want to explore the landscape defined by the energy of the pattern: we want to determine whether there are local energy minima, or whether the cell configuration can spontaneously relax towards equilibrium through a steady descent along its energy gradient. As the landscape is complicated, we must use computer simulations. We thus simulate the evolution of a collection of cells, following a deterministic gradient descent, according to eqns (6) and (7). Once we understand better the effect of energy minimization on cell rearrangement, we intend to include in future articles other phenomena which play a role in cell rearrangement: thermal fluctuations, chemotaxy, or exploration of neighbors by active protrusions.

Efficient 3D computations using Dirichlet tiling are possible (e.g. Tanemura *et al.*, 1983), but for simplicity we investigate only 2D patterns (a plane section of 3D Dirichlet domains is not a 2D Dirichlet tiling). Since 3D allows more degrees of freedom for topological rearrangement, it is likely that whatever cell rearrangement occurs in 2D also occurs in 3D.

Biological cases of cell rearrangement related to cell adhesion which can be approximated as 2D include the compaction and rounding of a homogeneous aggregate, or tissue healing; in heterogeneous aggregates, dispersal, mixing, sorting and engulfment (Graner, 1993). We do not consider specifically 3D problems like cylinder elongation (Mittenthal & Mazo, 1983) or gastrulation (Odell *et al.*, 1981). We do treat free boundaries, which simulate an aggregate suspended in a culture medium (e.g. Steinberg, 1963). A cell monolayer on an homogeneous substrate is quasi two-dimensional‡, with an adhesion energy depending on its domain perimeter (Steinberg & Garrod, 1975); seen from the top it has free boundaries, and the adhesion energy between cells and substrate can be incorporated in the energy associated with the bulk of each domain.

The surface energies e_{iM} and e_{ij} can, in principle, be experimentally measured, but not derived from microscopical mechanisms (for a discussion, see Bongrand, 1988; Curtis & Lackie, 1991; Graner, 1993). The hierarchy of the e_{iM} and e_{ij} determines the effect of cell adhesion; the relative values of the e_{iM} and e_{ij} determine the actual configurations obtained, while their absolute values and the dissipation only affect the time scale of the relaxation.

On the other hand, the stabilizing term E_{stab} must be determined with care to avoid any change in cell rearrangement. We consider 2D elastic membranes, whether stretched or compressed, their perimeter length L returns to a fixed value L_0. We chose $E_{\text{stab}} = 1/2\kappa(L-L_0)^2$; but we also used $E_{\text{stab}} = 1/2\kappa_{\text{bulk}}(A-A_0)^2$, where A is the bulk area of a 2D cell: it does not affect the simulations of shape and position rearrangement once E_{stab} is fixed consistently with surface energies (Appendix B).

Our initial conditions use cells either aligned or randomly dispersed. For random dispersal we chose cell shapes to be close to equilibrated shapes, using an excluded volume procedure; two centers cannot be closer than a fraction of R. Alternatively, the initial cell positions can be the result of an equilibration. For aligned cells, we introduce small random fluctuations in their initial position to avoid four-cell vertices. Except as noted, the simulations we present are robust to different initial conditions.

We use a flexible time step to ensure a smooth rearrangement, even near the singularities of the energy landscape (Appendix C). Instead of the number of time steps, we record the integrated elapsed time. To define the time scale, we express all the surface energies as a function of an energy scale E_0 and fix the dissipation. If μ_f is the normal fluid viscosity used in hydrodynamics (Appendix D), the time scale τ_0 is:

$$\tau_0 = \frac{\mu_c R}{E_0} = \frac{\mu_f R^2}{E_0}. \tag{8}$$

We use $R \sim 10^{-3}$ cm and the direct measure by Gordon *et al.* (1972) of $\mu_f/E_0 \approx 10^{-6}$ cm sec^{-1}, so τ_0 is of the order of 1000 sec. It would be 10–100 sec if $\mu_f \approx 10^3$

‡ Neighbor exchange in a monolayer is really a 3D process: former neighbors can still remain in apical contact when future neighbors have established a basal contact. The transitory four-cell vertex moves vertically along the apico-basal axis: either because of cell protrusion, intrinsically oriented (Jacobson *et al.*, 1986) or triggered by apico-basal positional information (Fristrom, 1988), or under the effect of surface adhesion.

poise, as Evans (1983) estimates for white blood cell cytoplasm and E_0 of the order 10^{-1}–10^{-2} erg cm^{-2} (Bell, 1988).

3.2. APPLICATION TO HOMOGENEOUS PATTERNS

With only one type of cell, say "dark" (d), there is a competition between the two surface energies e_{dd} and e_{dM}, quantified by the surface tension $\gamma_{dM} = e_{dM} - e_{dd}/2$ [Fig. 4(a) and (b)]. Except for the trivial case where $e_{dM} < e_{dd}/2$ and cells do not adhere (Fig. 5), γ_{dM} is positive and cells decrease their total interface with the medium. A loose aggregate compacts and most intercellular gaps shrink (Fig. 6). Single cell removal from an epithelium (Honda, 1983) results in healing by increasing the

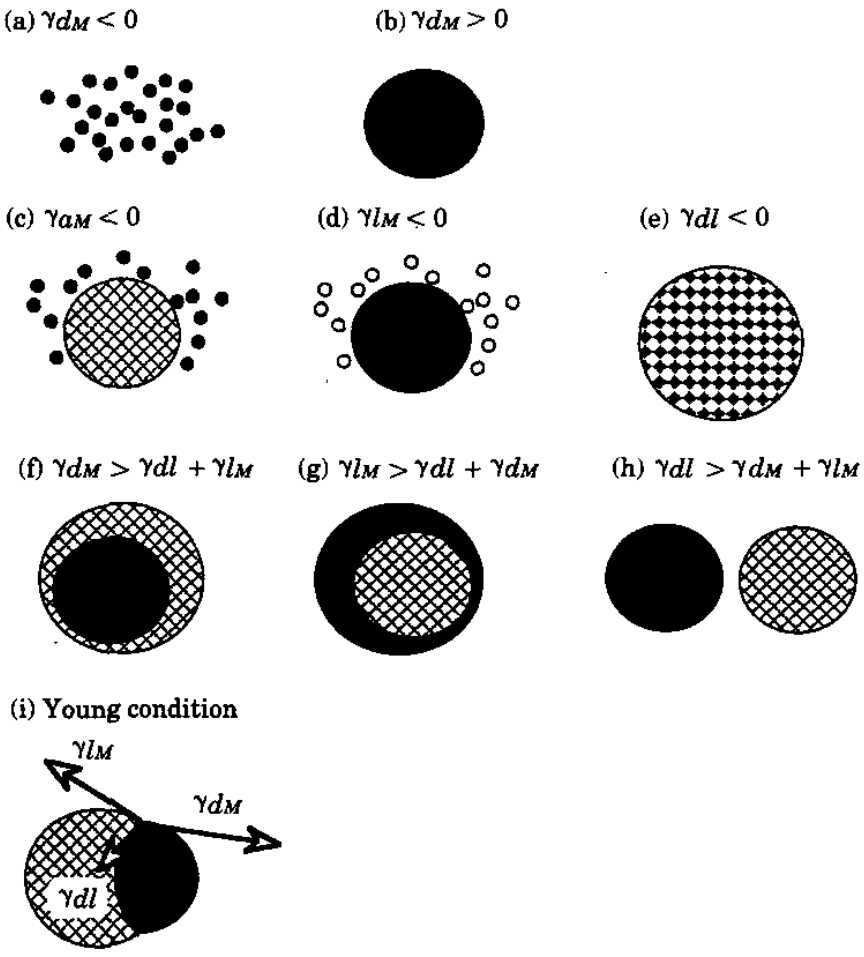

FIG. 4. Surface tensions [eqn (9)] determine the configuration with the minimum global energy. (a)–(b) With one type of cell, two cases occur: dispersal and cohesion. (c)–(e) With two types of cells and at least one negative surface tension: cells disperse, or mix into a checkerboard. (f)–(h) If one surface tension is greater than the sum of the others, the corresponding interface vanishes at equilibrium. (i) Between these extremes, the three interfaces d–l, d–M and l–M are stable and meet along a triple contact line. Their three radii are determined by their contact angle and the proportion of dark and light cells. All these configurations are experimentally observed, but (e)–(i) are dependent on initial conditions, and metastable cases also occur (from Graner, 1993). (□), Medium; (■), cohesive (d) cells; (■), weak (l) cells.

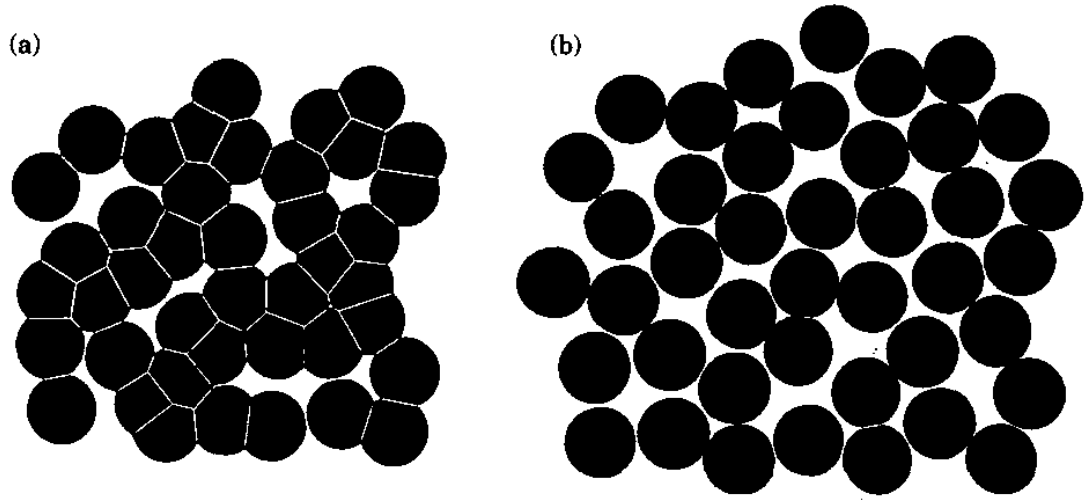

FIG. 5. Case of negative cell-medium surface tension. (a) A loose aggregate, similar to Fig. 9(a), with one cell type; (b) after ≈ 2 min ($0{\cdot}12\tau_0$) the cells have separated. Here, $e_{dd} = -5E_0$ and $e_{dM} = -3E_0$, $\gamma_{dM} = -0{\cdot}5E_0$.

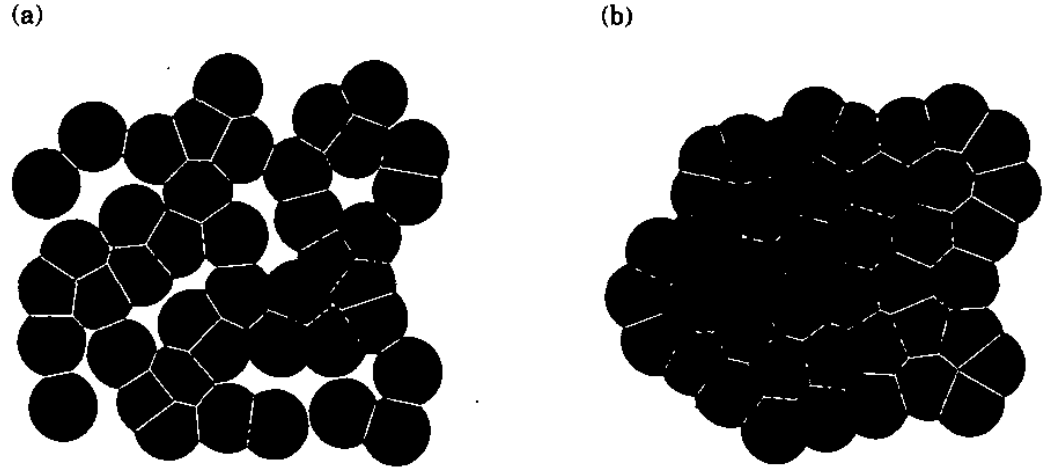

FIG. 6. Compaction of an aggregate. (a) The same loose initial conditions as in Fig. 5, and the same e_{dd}. The only change is the suppression of the cell-medium energy $e_{dM} = 0$, i.e. $\gamma_{dM} = 2{\cdot}5E_0$. (b) After ≈ 6 min ($0{\cdot}35\tau_0$), cell positions and shapes have relaxed and the interface length has decreased.

cell–cell contact length (Fig. 7). In the absence of any substrate, other tissues or adhesivity gradients within the cells, the minimum energy configuration corresponds to a minimum interface with the external medium and can be reached under adhesive driving (Fig. 8). The shape of the cells also relaxes. As expected for a surface-energy driven system, the average number of sides per cell within the bulk is six§; and as the perimeter length is constrained, few-sided and many-sided cells are almost non-

§ In 2D, a four-cell vertex has a longer perimeter than two three-cell vertices and decays; only three-cell vertices are stable (e.g. Gardner, 1986). Each edge is shared by two cells, so $N_{\text{edges}} = N_{\text{cells}}\langle n\rangle/2$. Each cell has on average $\langle n\rangle$ vertices, each shared by three cells, so $N_{\text{vertices}} = N_{\text{cells}}\langle n\rangle/3$. The Euler relation states that $N_{\text{vertices}} - N_{\text{edges}} + N_{\text{cells}} = 1$, and gives: $N_{\text{cells}}(\langle n\rangle/3 - \langle n\rangle/2 + 1) = 1$. In the limit of a large system $\langle n\rangle/6 \approx 1$ (Graustein, 1931).

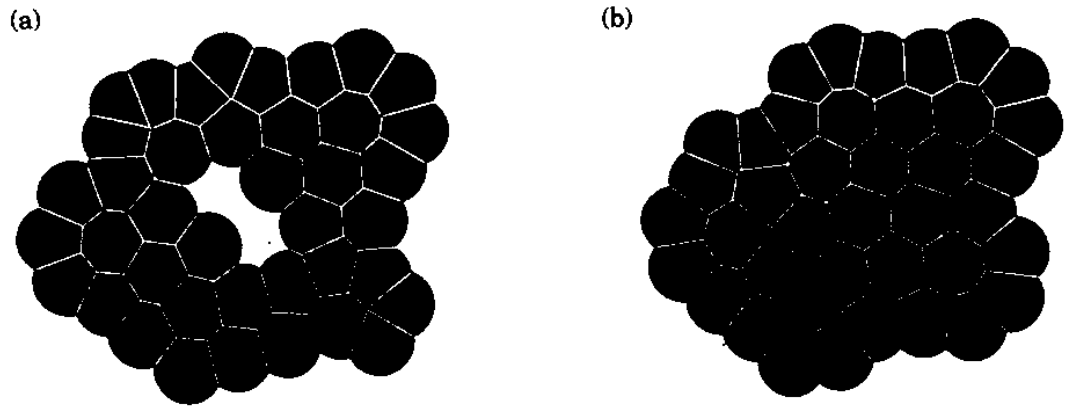

FIG. 7. Individual cell removal. (a) The same compact aggregate as in Fig. 6(b), from which two cells have been removed. Surface energies are the same. (b) After ≈ 5 min ($0{\cdot}32\tau_0$), cells from the margin relax into the empty space and cover it, while external cells barely move.

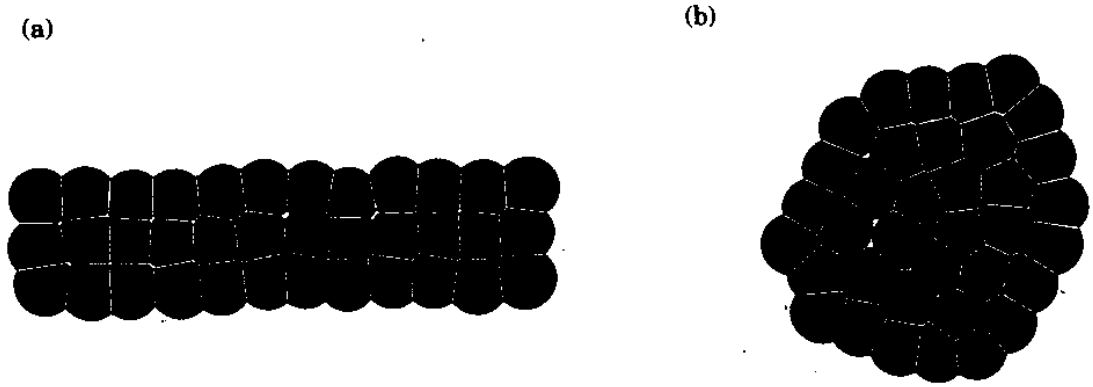

FIG. 8. Rounding of a long column. (a) Artificial initial conditions, same surfaces energies as in Figs 6 and 7. (b) After ≈ 3 hr ($11{\cdot}6\tau_0$), cells move over distances much longer than their diameter.

existent. The distribution of side numbers is very narrow, with almost all cells penta-, hexa- or heptagons (Glazier, 1989). As in biological patterns (Honda & Eguchi, 1980), a perfect hexagonal pattern is seldom reached since it requires either selective deletion of ill-placed cells (Cagan & Ready, 1989), rare initial conditions (Herdtle & Aref, 1991), or that cells explore all the available configurations. Surface energy minimization does not require that cells be isometric (Lewis, 1948; Smith, 1954; Honda, 1983).

3.3. CELL MIXTURES

Mixtures of two types of biological cells lead to various final states such as dispersal (Mège, 1991), checkerboard patterns (Honda *et al.*, 1986), total or partial cell-sorting and engulfment (Steinberg, 1963, 1970; Armstrong, 1989). We chose different values for the surface energies to simulate these observations and to determine the possible relative cell adhesivities.

Surface tensions γ are the differences in energy between a heterotypic interface and the homotypic interface that the same membrane portion could establish. They have an intuitive significance, they determine the minimum energy configuration of the macroscopic interface. With two cell types we define "dark" (d) cells as more cohesive than "light" (l) cells if $e_{dd} < e_{ll} < 0$. The three surface tensions γ_{dl}, γ_{dM}, γ_{lM} are (Graner, 1993):

$$\gamma_{dl} = e_{dl} - \frac{e_{dd}+e_{ll}}{2}, \tag{9a}$$

$$\gamma_{dM} = e_{dM} - \frac{e_{dd}}{2}, \tag{9b}$$

$$\gamma_{lM} = e_{lM} - \frac{e_{ll}}{2}. \tag{9c}$$

Usually, we take e_{dM} and e_{lM} as equal to zero, leaving three free parameters. If so, the behavior of the system is described by one dimensionless parameter quantifying the relative energy costs, $\gamma_{dl}/(\gamma_{dM}-\gamma_{lM})$, negative when $e_{dl} < (e_{dd}+e_{ll})/2$, and greater than one when $e_{dl} > e_{ll}$. We present one set of typical adhesion parameters for each case (Fig. 4).

3.3.1. *Case:* $e_{dl} < (e_{dd}+e_{ll})/2 < 0$

If the cost of a heterotypic d-l contact is less than the average of the homotypic contacts, γ_{dl} is negative and cells intermingle. Such mixing, which occurs during the sexual maturation of avian oviduct, has been analyzed by Honda *et al.* (1986). Using their surface energy values we simulate the evolution of a checkerboard pattern (Fig. 9).

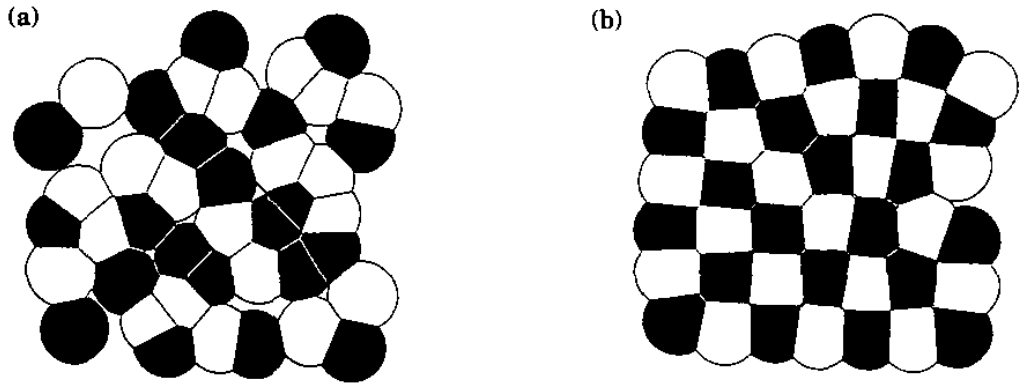

FIG. 9. Checkerboard pattern. Relative values of the energies obey the relation determined by Honda *et al.* (1986) for avian oviduct, $e_{dl}-e_{dd} \approx -[e_{ll}-e_{dd}]$, corresponding to a negative γ_{dl}. (a) Initial conditions sufficiently close to the final state (see text). (b) After ≈ 45 sec ($0{\cdot}045\tau_o$), cells intermingle. A defect creates a deformation in the checkerboard extending over a few cell diameters. Surface energies are $e_{dM} = e_{lM} = 0$; $e_{dd} = -3E_o$; $e_{dl} = -4E_o$; $e_{ll} = -2E_o$. Corresponding surface tensions are $\gamma_{dM} = 1{\cdot}5E_o$, $\gamma_{dl} = -1{\cdot}5E_o$, $\gamma_{lM} = E_o$.

This original case where γ_{dl} is negative shows some essential physical features of surface energy-driven patterns. The minimization of surface energy tends to decrease the homotypic interface and to create a periodic pattern of four-sided, roughly square cells of alternating type. But when the differential adhesion brings two three-cell vertices near each other they oscillate around a singularity, since a four-cell vertex is unstable. An array of four-sided cells is unstable and decays into a pattern with a wide side number distribution, from tetragons to octagons, as observed experimentally.

This instability, which affects numerical simulations (Honda *et al.*, 1986), arises from the shape of the energy landscape. Arbitrary initial conditions usually result in a large number of defects, whose effect extends a few cell diameters inside the pattern. The initial state of avian oviduct is not arbitrary. We must select an initial condition near the desired pattern. We show a picture with one weakly metastable defect [Fig. 9(b)].

The experimental checkerboard pattern, alternating big and small cells, cannot be represented by standard Dirichlet domains. Since membranes are the mediatrices between two neighboring centers, they are necessarily regularly spaced to represent a strictly periodic pattern of dark and light cells, so all the cells have the same size. By relaxing the constraint on R, however, our free Dirichlet domains could account for two different fixed cell sizes R_d and R_l [Fig. 3(a)]. When two neighboring centers i, j are separated by r_{ij}, instead of fixing the membrane position at a distance $x_i = x_j = r_{ij}/2$ from both centers, we could consistently define x_i and x_j as:

$$x_i + x_j = r_{ij}, \tag{10a}$$

$$R_i^2 + x_i^2 = R_j^2 + x_j^2. \tag{10b}$$

3.3.2. *Case:* $(e_{dd}+e_{ll})/2 < e_{dl} < e_{ll}+(e_{dM}-e_{lM})$

In this case, γ_{dl} is positive and the total energy is lower if cells are sorted into homogeneous clusters. Moreover, $\gamma_{dM} > \gamma_{lM}+\gamma_{dl}$, the d–M interface is unstable and dark cells tend to sort inwards. Since an l–l cell contact is more costly than a d–l one, itself more costly than a d–d one, two dark cells can contact without having to overcome any potential energy barrier. More precisely, there is no interaction between two distant cells and their relative movement is energetically neutral. If, during the rearrangement of the whole pattern, two initially distant dark cells contact, then their infinitesimal contact surface increases spontaneously. In addition, if we included thermal fluctuations in the cell positions, cells would diffusively perform such energetically neutral movements (Graner, 1993). Similarly, three dark cells can expel a light cell. Simulations display this spontaneous sorting by neighbor exchange. We present an example where $e_{dd}.e_{ll} \approx (e_{dl})^2$, as in the speculative "site-density model", where adhesivities are determined by the surface density of adhesion sites (Steinberg, 1963, 1975).

To emphasize the effect of surface energies, Fig. 10 starts with the same loose aggregate as Fig. 9. Cohesive dark domains coalesce and a light monolayer forms, leading to a totally sorted configuration. This sorting also occurs for tight, gapless

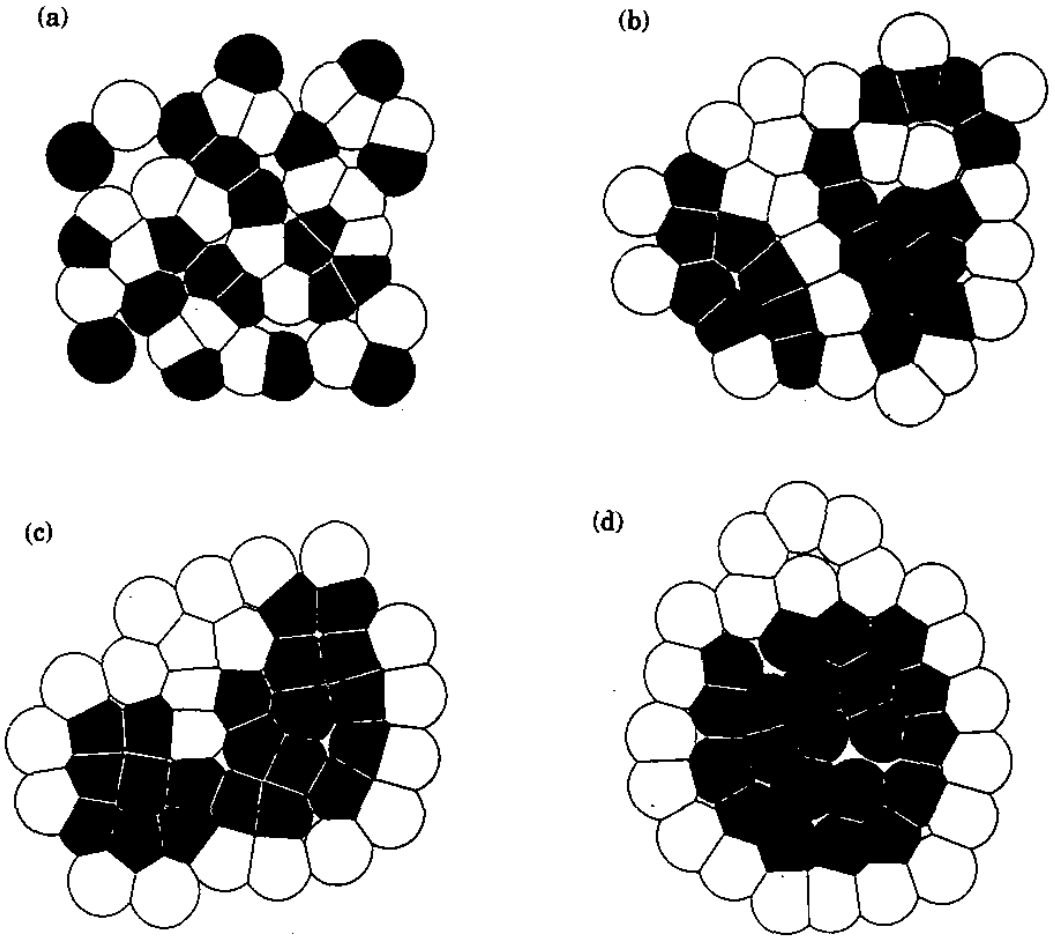

FIG. 10. Complete cell-sorting. (a) Initial configuration: the same loose aggregate as in Fig. 9. (b) $\approx$4 min ($0{\cdot}22\tau_o$), cohesive dark cells cluster. (c) $\approx$10 min ($0{\cdot}60\tau_o$), dark clusters coalesce and light cells fill the external monolayer. (c) $\approx$1 hr ($4{\cdot}0\tau_o$), sorted dark and light clusters complete their rounding. Surface energies are chosen so that $e_{dd} \cdot e_{ll} \approx (e_{dl})^2$: $e_{dM} = e_{lM} = 0$; $e_{dd} = -12E_o$; $e_{dl} = -5E_o$; $e_{ll} = -2E_o$. Corresponding surface tensions are $\gamma_{dM} = 6E_o$, $\gamma_{dl} = 2E_o$, $\gamma_{lM} = E_o$.

initial conditions (Fig. 11), showing that adhesion alone can drive experimentally observed long-distance cell rearrangement (for a review see Steinberg, 1970; Armstrong, 1989).

In the checkerboard, each cell relaxed among its neighbors within a short time. But during what we define as "long distance rearrangement", some cells, initially very distant (separated by many cell diameters), happen to come into contact‖. Cells that are 2D are stiffer than 3D cells and intercalate less easily between neighbors;

‖ To distinguish short-range from long-range rearrangement, this criterion is usually more relevant than requiring that two initially close cells separate. During tissue growth and cell division, as in *Fundulus* epiboly (Trinkaus, 1984; Keller & Trinkaus, 1987), cells initially in contact are finally spread over the whole egg surface without any large-scale movement relative to their neighbors. In tissue elongation and narrowing, for example, during sea urchin gastrulation (Ettensohn, 1984; Hardin, 1987), local rearrangement allows convergence of cells initially slightly separated on the same axial level, and cell divergence along the elongating archenteron axis. But convergence of cells in arbitrary directions results either from unlikely tissue shrinking, or from global rearrangement where neighboring cells have independent trajectories.

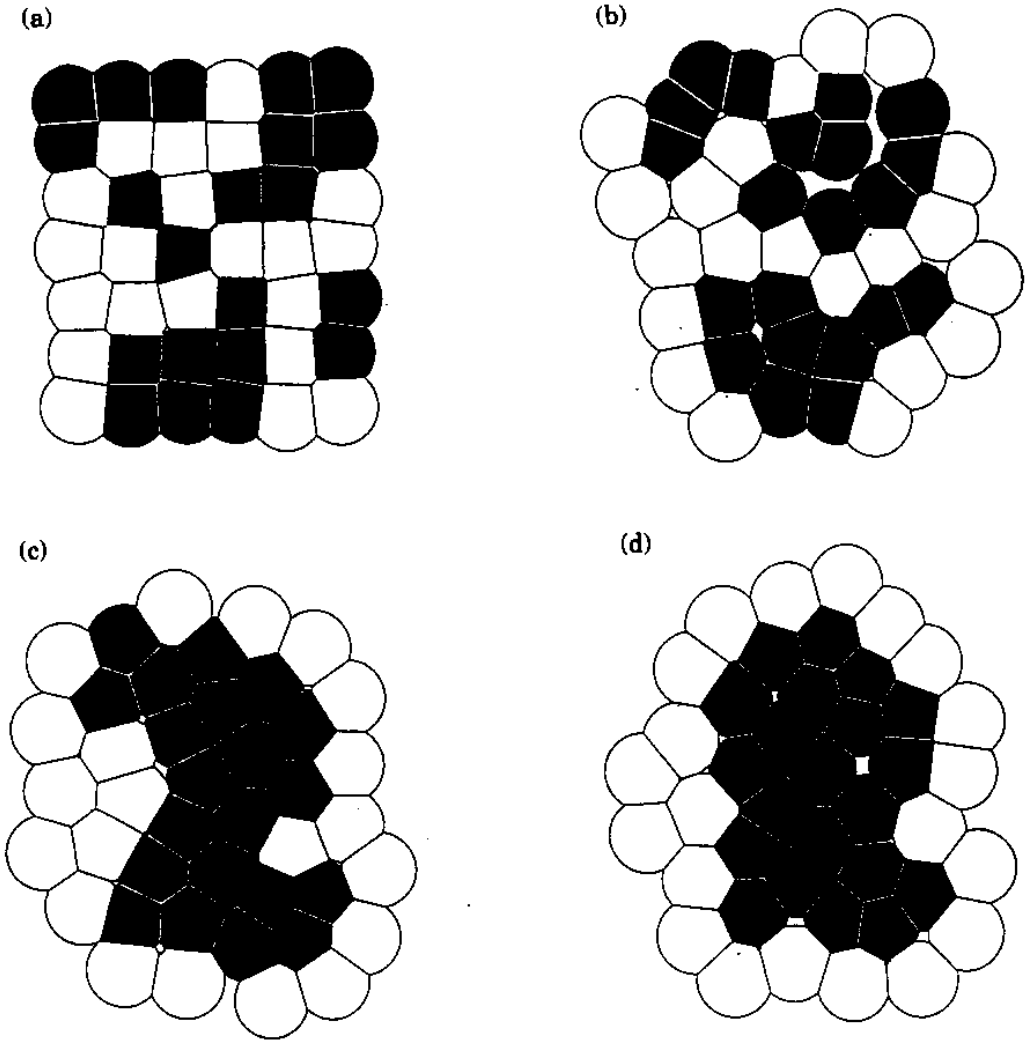

FIG. 11. Cell-sorting in a compact aggregate. (a) Artificial initial conditions, same energies as in Fig. 10. (b) $\approx$6 min (0·36τ_o); (c) $\approx$11 min (0·67τ_o); (d) $\approx$15 min (0·93τ_o). Cells are sorted, rounding is not complete yet.

symmetries are more likely to create neutral or degenerate situations; for example, a cell submitted to a force on both sides feels a resulting zero force. In such case, our strictly deterministic model does not break the symmetry and the Dirichlet domain remains pinned; while a real cell would actually move, although the energy landscape is nearly flat. However, the discrete time step allows cells to ignore some small flat energy regions (Appendix C).

The same surface energies simulate the engulfment of a cohesive dark aggregate by a less cohesive light one (Fig. 12), with the same final state as cell-sorting (Townes & Holtfreter, 1955; Steinberg, 1970; Armstrong, 1989). Dark cells tend to decrease their interface with the culture medium, as a *d–l* contact is less costly. The triple contact point is out of equilibrium (since the Young condition is not satisfied) as are the high curvature regions. Since only a few points along the outer boundary drive the long-distance cell movements, rearrangement is slow. The same reason slows the rounding of a stretched aggregate (Fig. 8).

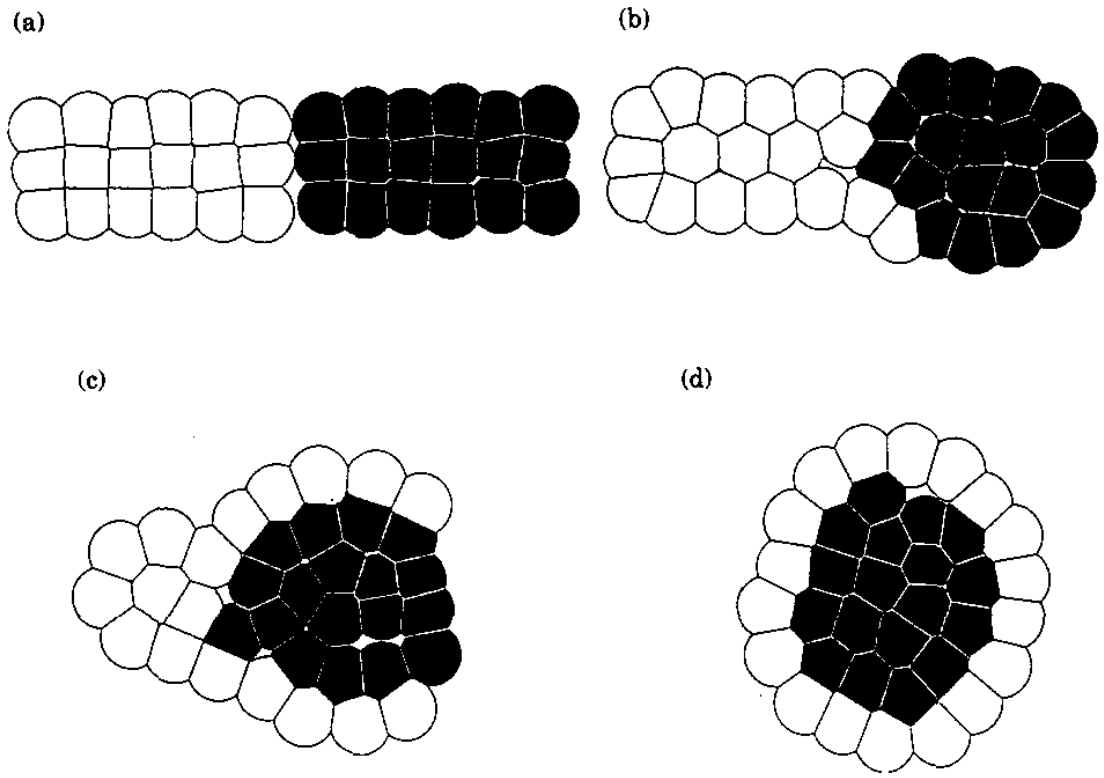

FIG. 12. Engulfment. (a) Initial conditions: two homogeneous aggregates are in contact, same energies as in Figs 10 and 11. (b) $\approx$9 min ($0{\cdot}56\tau_o$), the dark–light contact length increases. (c) $\approx$45 min ($2{\cdot}6\tau_o$), dark–medium interface decreases and light–medium interface increases. (d) $\approx$2 hr ($7{\cdot}1\tau_o$), rounding is complete and the final state is similar to Fig. 10(d).

3.3.3. *Case:* $(e_{dd}+e_{ll})/2 < e_{dl} < e_{dd}+(e_{lM}-e_{dM})$

If the surface energy with the medium is different for both the two types of cells, for example, due to their hydrophily or hydrophobicity (Davis, 1984; Bongrand, 1988), we can observe "position reversal" [Fig. 13(a)–(c)]. Indeed, if $e_{lM}-e_{dl} > e_{dM}-e_{dd}$ (i.e. $\gamma_{lM} > \gamma_{dM}+\gamma_{dl}$), the cohesive dark cells no longer have the highest surface tension with the culture medium; at equilibrium they surround the light cells (Phillips & Davis, 1978). However, the final state is sensitive to initial conditions [Fig. 13(a')–(c')], and a metastable state can appear (Graner, 1993) since dark cell clusters, which are never in contact with the culture medium, have no opportunity to sort outwards (Armstrong & Armstrong, 1984).

3.3.4. *Case:* $e_{ll}+(e_{dM}-e_{lM}) < e_{dl} < (e_{dM}+e_{lM})$

If a *d–l* contact is more costly, γ_{dl} is large enough that it is possible to satisfy the Young condition. The equilibrium state consists of a triple contact between the medium, a dark and a light cluster. If transitory heterotypic contacts are too costly to allow neighbor exchange, sorting does not occur spontaneously. Thus, already formed clusters round, but there is no effective attraction between dark cells to make clusters coalesce (Fig. 14).

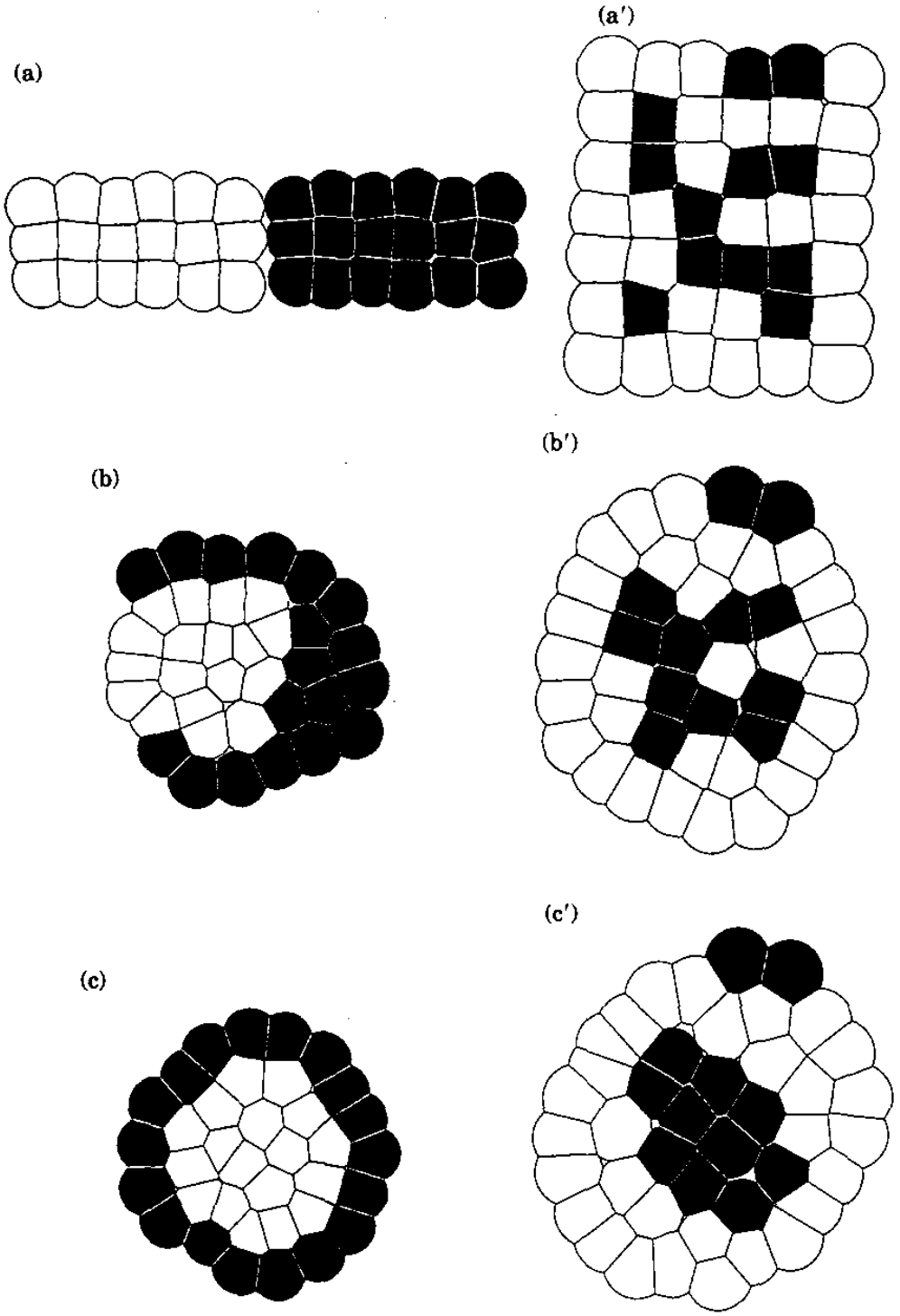

FIG. 13. "Position reversal". Cell–cell energies are the same as in Fig. 10, but light–medium interface has a high energy, so that $\gamma_{lM} > \gamma_{dM} + \gamma_{dl}$. This situation is sensitive to initial conditions (Armstrong & Armstrong, 1984, see text). (a) Same initial conditions as in Fig. 12. (b) $\approx$20 min ($1{\cdot}3\tau_o$), light–medium interface decreases. (c) $\approx$3·5 hr ($13\tau_o$), a lower energy state is reached. The respective position of the cells is not related to their cohesiveness (Phillips & Davis, 1978). (a') Artificially selected initial conditions. (b') $\approx$1 min ($0{\cdot}071\tau_o$). The more cohesive dark cells cluster and are totally surrounded by light cells. Dark cells in contact with the medium sort outwards. (c') $\approx$12 min ($0{\cdot}72\tau_o$). Cells reach a metastable state (Graner, 1993). In both simulations, $e_{dM} = E_o$; $e_{lM} = 9E_o$. As above, $e_{dd} = -12E_o$, $e_{dl} = -5E_o$, $e_{ll} = -2E_o$. Corresponding surface tensions are $\gamma_{dM} = 7E_o$, $\gamma_{dl} = 2E_o$, $\gamma_{lM} = 10E_o$.

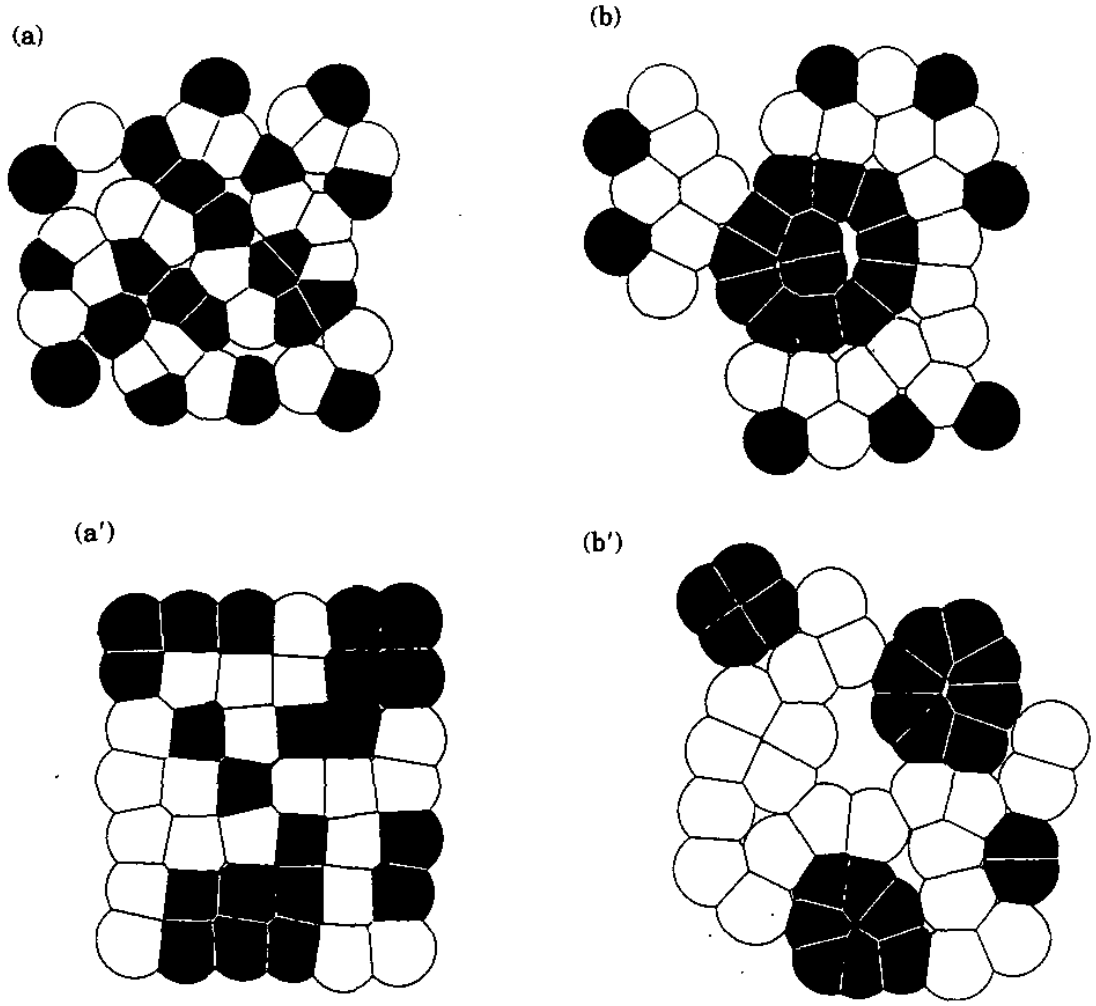

FIG. 14. Partial cell-sorting. Identical to Figs 10 and 11, except that e_{dl} is larger than both e_{dd} and e_{ll}. The lower energy state is determined by the Young condition, but potential energy barriers can create metastable states. (a) Same loose initial conditions as in Fig. 10. (b) ≈ 11 min ($0{\cdot}68\tau_o$). Cells remain pinned and no longer sort spontaneously. (a') Same tight initial conditions as in Fig. 11. (b') ≈ 15 min ($0{\cdot}90\tau_o$), light cells tend to surround dark cell clusters which remain separated. In both simulations, $e_{dl} = -E_o$; as above, $e_{dM} = e_{lM} = 0$, $e_{dd} = -12E_o$, $e_{ll} = -12E_o$. Corresponding surface tensions are $\gamma_{dM} = 6E_o$, $\gamma_{dl} = 6E_o$, $\gamma_{lM} = E_o$.

FIG. 15. Dispersal, e_{dl} is high, so that $\gamma_{dl} > \gamma_{dM} + \gamma_{lM}$. (a) Initial conditions without homotypic contacts. (b) ≈ 2 min ($0{\cdot}14\tau_o$), heterotypic contacts are replaced by cell–medium interfaces. Here, $e_{dl} = E_o$; as above, $e_{dM} = e_{lM} = 0$, $e_{dd} = -3E_o$, $e_{ll} = -2E_o$. Corresponding surface tensions are $\gamma_{dm} = 1{\cdot}5E_o$, $\gamma_{dl} = 3{\cdot}5E_o$, $\gamma_{lM} = E_o$.

3.3.5. *Case:* $(e_{dM}+e_{lM})<e_{dl}$

If one surface tension is greater than the sum of the others, as in case (b), the corresponding interface vanishes and no triple point exists. If $e_{dl}>e_{dM}+e_{lM}$ or equivalently $\gamma_{dl}>\gamma_{dM}+\gamma_{lM}$, the aggregate dissociates (Mège, 1991). Evolution is quick, as rearrangements are short-range (Fig. 15).

4. Discussion

4.1. CRITIQUE OF THE MODEL

Our model was designed to study the effects of differential adhesion on cellular patterns. Does it determine the energy landscape in which the cells move?

Each cell is represented by one point, its Dirichlet center. After defining the total adhesion energy of the pattern, we take its gradient with respect to a subset of the infinity of all position variables. Thus, we do not explore all possible ways by which cells can intercalate and move. But cells can rearrange by continuously going down the gradient of their adhesion energies, and real cells can probably do so more easily than in our simulations. Cellular patterns can rearrange and sort under adhesion.

Our simulations have some numerical limitations. The discrete time steps can create oscillations in numerically unstable cases (Appendix C) and the finite number of geometrical parameters constrains the shapes and gaps (Appendix B). 3D simulations with a large number N of cells are possible (Appendix C), but an extended Potts model is more appropriate for a quantitative characterization of cell-sorting (Graner & Glazier, 1992) and a discussion of the possible role of fluctuations (Glazier & Graner, 1993). Biological cell-sorting typically involves 10^5–10^6 cells and, although cells rearrange more easily in 3D space, they do not always reach the minimal energy state, even if $(e_{dd}+e_{ll})/2<e_{dl}<e_{ll}$ (Steinberg, 1975; Sulsky *et al.*, 1984; Graner, 1993).

4.2. RELEVANCE TO BIOLOGICAL CELLS

Biological cell surfaces are usually adhesive, and driving by adhesion can thus be a general morphogenic mechanism. Other physical phenomena may be involved as well (Newman & Comper, 1990). For loose aggregates, Brownian motion (Graner, 1993) and residual convective flows in the culture medium can create random cell movements.

Biological mechanisms can co-operate to make a cell move (Oster *et al.*, 1983), for example, cell rearrangement is accompanied by amoebal-like deformations (Oster, 1984; Keller & Hardin, 1987; Oster & Perelson, 1987; Weliky & Oster, 1990). There is evidence that cellular actin-rich extensions (Oster, 1984; Jacobson *et al.*, 1986; Armstrong, 1989) and contractile actin microfilaments (Owaribe *et al.*, 1981; Owaribe & Masuda, 1982; Fristrom, 1988) could influence morphogenesis (Ettensohn, 1985).

For most cells the visible local protrusions or contractions in cell shape reflect the cell's internal activity. However, observed deformations could sometimes be a consequence of cell movements (Honda *et al.*, 1982; Kolega, 1986), for example, when

cell motility has been inhibited. Trinkaus *et al.* (1992) showed that 100% of an observed cell population could undergo directed movements during *Fundulus* gastrulation. However, they raised two issues. First, contact-inhibited filo-lamellipodial cells moved. Second, after cell division, daughter cells resumed their mother's movement within a time too short to account for rearrangement of their locomotile apparatus.

Both phenomena and other surprising observations are clearly compatible with relaxation under surface adhesion (Glazier *et al.*, 1993, in press); for example, the decrease in the number of marginal enveloping layer cells during *Fundulus* epiboly¶, the non-isometricity of biological cells (section 3.2), or the large mobility of marginal cells during wound healing and the slowing down of cells' velocities when the wound is closed (Graner, 1993). Adhesion provides an intuitive explanation, especially when cells can rearrange without having to overcome any potential energy barrier.

5. Conclusion

We have examined the effect on biological cell movement of a deterministic force based on the gradient of the cell–cell adhesion energy, using a flexible geometrical model based on free Dirichlet domains. The model naturally treats the cell geometry in rearrangement. It also describes cell boundaries, intercellular gaps and surface adhesion. Both surface energies and surface tensions affect the global tissue organization.

We have implemented a two-dimensional simulation and studied the effects of discretization on our computations. We simulated aggregation and rounding of a cell collection and aggregate dissociation, both of which involve only short-distance rearrangement. We could also simulate the checkerboard pattern of sexually maturing avian oviduct. Long-distance movements under differential adhesion can also reproduce aggregate engulfment and total and partial cell-sorting with the correct time scale. "Positional reversal" is also possible.

We have thus shown that rearrangement of both passive and active cells can be driven by the adhesion energy of the total cell collection alone. Adhesivity is a general feature of cell surfaces and it offers a coherent view of morphogenetic phenomena for both cells and tissues.

We are indebted to J. A. Glazier, H. Honda, M. Sato and M. Weliky for valuable help and fruitful discussions. This research has been financially supported by the Inoue Foundation, J.S.P.S., Monbusho.

¶ During *Fundulus* epiboly the margin of the epithelial enveloping layer, pulled by the underlying yolk syncytial layer, spreads over an increasing portion of the egg (Keller & Trinkaus, 1987; Weliky & Oster, 1990). If the global epithelium was relaxing its total energy, the observed decrease of marginal cell number would be much less surprising and cells at the boundary would not need be functionally different from the others. Indeed, we could interpret the decrease by the following geometrical packing argument. The surface S of a spherical cap of radius r and polar angle θ is $S = 2\pi r(1-\cos\theta)$, its perimeter $P = 2\pi r \sin\theta$. When cells relax, if we consider N square cells uniformly tesselating this cap, the cell side a is determined by the average available space, i.e. $a^2 = S/N$. The number of cells at the margin is $n = P/a$, so that $n^2 = P^2N/S = 2\pi N(1+\cos\theta)$; n is slightly greater if cells are stretched along the meridian by the traction of the yolk. This function is strictly decreasing when θ increases, although P is increasing during the first half of epiboly.

REFERENCES

ANTONELLI, P., ROGERS, T. & WILLARD, M. (1973). Geometry and the exchange principle in cell aggregation kinetics. *J. theor. Biol.* **41,** 1–21.

ARMSTRONG, P. B. (1989). Cell sorting out: the self-assembly of tissues *in vitro*. *Crit. Rev. Biochem. molec. Biol.* **24,** 119–149.

ARMSTRONG, P. B. & ARMSTRONG, M. T. (1984). A role for fibronectin in cell-sorting. *J. Cell Sci.* **69,** 179–197.

BELL, G. I. (1988). Models of cell adhesion involving specific binding. In: *Physical Basis of Cell–Cell Adhesion* (Bongrand, P., ed.) pp. 227–258. Boca Raton, FL: CRC Press.

BÉNARD, H. & DAUZÈRE, C. (1913). Tourbillons cellulaires isolés. *Films pédagogiques Gaumont.*

BONGRAND, P. (ed.). (1988). *Physical Basis of Cell–Cell Adhesion.* Boca Raton, FL: CRC Press.

BREDIN, J.-D. (1988). Rapport Thouret, September 29th, 1789. In: *Sieyès.* Paris: De Fallois.

CAGAN, R. L. & READY, D. F. (1989). The emergence of order in the *Drosophila* pupal retina. *Develop. Biol.* **136,** 346–362.

CARTER, S. (1967). Haptotaxis and the mechanism of cell motility. *Nature, Lond.* **213,** 256–260.

CHILDRESS, S. & PERCUSS, J. K. (1981). Modeling of cell and tissue movements in the developing embryo. *Lect. math. Life Sci.* **14,** 59–88.

CURTIS, A. S. & LACKIE, J. M. (ed.). (1991). *Measuring Cell Adhesion.* England: Wiley.

DAVIS, G. S. (1984). Migration-directing liquid properties of embryonic amphibian tissues. *Am. Zool.* **24,** 649–655.

ETTENSOHN, C. A. (1984). Primary invagination of the vegetal plate during sea urchin gastrulation. *Am. Zool.* **24,** 571–588.

ETTENSOHN, C. A. (1985). Mechanisms of epithelial invagination. *Q. Rev. Biol.* **60,** 289–307.

EVANS, E. (1983). Structural model for passive granulocyte behavior based on mechanical deformation and recovery after deformation tests. In: *White Blood Cell Mechanics: Basic Science and Clinical Aspects* (Lichtman, F. & Meiselman, B., eds) p. 53. New York: Alan R. Liss.

FRASER, S. E. (1985). Cell interactions involved in neuronal patterning: an experimental and theoretical approach. In: *Molecular Basis of Neural Development* (Edelman, G. M., Gall, W. E. & Cowan, W. M., ed.) p. 481. New York: Wiley.

FRISTROM, D. K. (1988). The cellular basis of epithelial morphogenesis. A review. *Tissue Cell* **20,** 645–690.

FROST, H. J. (1991). Simulation of microstructural evolution in polycrystalline films. In: *Evolution of Thin Film and Surface Microstructure,* Vol. 202 (Thompson, C. V., Tsao, J. Y. & Srolovitz, D. J., eds). Boston: MA: MRS Symposia Proceedings.

GARDNER, M. (1986). Mathematical games. *Sci. Am.* **254,** 16–23.

GLAZIER, J. A. (1989). The dynamics of two dimensional cellular patterns. Ph.D. Thesis, Chicago, IL: University of Chicago.

GLAZIER, J. A. & GRANER, F. (1993). A simulation of the differential adhesion driven rearrangement of biological cells. *Phys. Rev. E* **47,** 2128–2154.

GLAZIER, J., GRANER, F., BERGE, B., MAGNASCO, N., MOLHO, P., FRADKOV, V. & UDLER, D. (1993). *Int. J. Mod. Phys. B.*, in press.

GOEL, N., CAMPBELL, R., GORDON, R., ROSEN, R., MARTINEZ, H. & YCAS, M. (1970). Self-sorting of isotropic cells. *J. theor. Biol.* **28,** 423–468.

GOEL, N. & LEITH, A. (1970). Self-sorting of anisotropic cells. *J. theor. Biol.* **28,** 469–482.

GOEL, N. & ROGERS, G. (1978). Computer simulation of engulfment and other movements of embryonic tissues. *J. theor. Biol.* **71,** 103–140.

GORDON, R., GOEL, N. S., STEINBERG, M. S. & WISEMAN, L. L. (1972). A rheological model sufficient to explain the kinetics of cell-sorting. *J. theor. Biol.* **37,** 43–73.

GRANER, F. (1993). Can surface adhesion drive cell-rearrangement? Part I: Biological cell-sorting. *J. theor. Biol.* **164,** 455–476.

GRANER, F. & GLAZIER, J. A. (1992). A two-dimensional extended Potts model for cell-sorting. *Phys. Rev. Lett.* **69,** 2013–2016.

GRAUSTEIN, W. C. (1931). On the average number of sides of polygons of a net. *Ann. Math.* **32,** 149–153.

GREENSPAN, D. (1981). A classical molecular approach to computer simulation of biological sorting. *J. math. Biol.* **12,** 227–235.

GUSTAFSON, T. & WOLPERT, L. (1963). The cellular basis of morphogenesis and sea urchin development. *Int. Rev. Cytol.* **15,** 139–214.

HARDIN, J. D. (1987). Archenteron elongation in the sea urchin is a micro-tubules independent process. *Develop. Biol.* **121,** 253–262.

HASEGAWA, M. & TANEMURA, M. (1976). On the pattern of space division by territories. *Ann. Inst. Stat. Math.* **28B**, 509–519.

HERDTLE, T. & AREF, H. (1991). Relaxation of fractal foams. *Phil. Mag. Lett.* **64**, 335.

HONDA, H. (1978). Description of cellular patterns by Dirichlet domains: the two-dimensional case. *J. theor. Biol.* **72**, 523–543.

HONDA, H. (1983). Geometrical models for cells in tissue. *Int. Rev. Cytol.* **81**, 191–248.

HONDA, H. & EGUCHI, G. (1980). How much does the cell boundary contract in a monolayered cell sheet? *J. theor. Biol.* **84**, 575–588.

HONDA, H., OGITA, Y., HIGUCHI, S. & KANI, K. (1982). Cell movements in a living mammalian tissue: long term observation of individual cells in wounded corneal endothelia of cats. *J. Morphol.* **174**, 25–39.

HONDA, H., YAMANAKA, H. & EGUCHI, G. (1986). Transformation of a polygonal cellular pattern during sexual maturation of the avian oviduct epithelium: computer simulation. *J. Embryol. exp. Morphol.* **98**, 1–19.

JACOBSON, A. G., OSTER, G. F., ODELL, G. & CHENG, L. (1986). Neurulation and the cortical tractor model for epithelial folding. *J. Embryol. exp. Morphol.* **906**, 19–49.

JOUANNEAU, J., TUCKER, G., BOYER, B., VALLÉS, A. & THIÉRY, J.-P. (1991). Epithelial cell plasticity in neoplasia. *Cancer Cell* **12**, 525–529.

KELLER, R. (1987). Review: cell rearrangement in morphogenesis. *Zool. Science* **4**, 763–779.

KELLER, R. E. & HARDIN, J. P. (1987). Cell behavior during active cell rearrangement: evidence and speculation. *Cell Behavior: Shape, Adhesion and Motility* (*J. Cell Sci. Suppl.*) (Heaysman, C. M. J. & Watt, F., eds) **8s**, 369–393.

KELLER, R. E. & TRINKAUS, J. P. (1987). Rearrangement of enveloping layer cells without disruption of the epithelial permeability barrier as a factor in *Fundulus* epiboly. *Develop. Biol.* **120**, 12–24.

KOLEGA, J. (1986). Effects of mechanical tension on protrusive activity and mirofilament and intermediate filament organization in an epidermal epithelium moving in culture. *J. Cell Biol.* **102**, 1400–1411.

LEITH, A. & GOEL, N. (1971). Simulation of movements of cells during self-sorting. *J. theor. Biol.* **33**, 171–188.

LEWIS, F. T. (1948). The analogous shapes of cells and bubbles. *Proc. A.A.A.S.* **77**, 147–186.

MARVIN, J. W. (1939). The shape of compressed lead shot and its relation to cell shape. *Am. J. Bot.* **26**, 280–288.

MATELA, R. J. & FLETTERICK, R. J. (1979). A topological exchange model for cell self-sorting. *J. theor. Biol.* **76**, 403–414.

MATELA, R. J. & FLETTERICK, R. J. (1980). Computer simulation of cellular self-sorting: a topological exchange model. *J. theor. Biol.* **84**, 673–690.

MATZKE, E. B. (1939). Volume–shape relationships in lead shot and their bearing on cell shapes. *Am. J. Bot.* **26**, 288–293.

MÈGE, R.-M. (1991). Les molécules d'adhérence cellulaire: molécules morphogénétiques. *Médecines/ Sciences* **7**, 544–552.

MITTENTHAL, J. E. & MAZO, R. M. (1983). A model for shape generation by strain and cell–cell adhesion in the epithelium of an arthropod leg segment. *J. theor. Biol.* **100**, 443–483.

NEWMAN, S. A. & COMPER, W. D. (1990). "Genetic" physical mechanisms of morphogenesis and pattern formation. *Development* **110**, 1–18.

ODELL, G. M., OSTER, G., ALBERCH, P. & BURNSIDE, B. (1981). The mechanical basis of morphogenesis. I. Epithelial folding and invagination. *Develop. Biol.* **85**, 446–462.

OSTER, G. (1984). On the crawling of cells. *J. Embryol. exp. Morphol.* **83s**, 329–364.

OSTER, G., MURRAY, J. D. & HARRIS, A. K. (1983). Mechanical aspects of mesenchymal morphogenesis. *J. Embryol. exp. Morphol.* **78**, 83–125.

OSTER, G. & PERELSON, A. (1987). The physics of cell motility. In: *Cell Behavior: Shape, Adhesion and Motility*, Vol. 8 (*J. Cell Sci. Suppl.*) (Heaysman, C. M. J. & Watt, F., eds) pp. 35–54.

OWARIBE, K., KODAMA, R. & EGUCHI, G. (1981). Demonstration of contractility of circumferential actin bundles and its morphogenetic significance in pigmented epithelium *in vitro* and *in vivo*. *J. Cell Biol.* **90**, 507–514.

OWARIBE, K. & MASUDA, H. (1982). Isolation and characterization of circumferential actin bundles from retinal pigmented epithelial cells. *J. Cell Biol.* **95**, 310–315.

PHILLIPS, H. M. & DAVIS, G. S. (1978). Liquid-tissue mechanics in amphibian gastrulation: germ-layer assembly in *Rana pipiens*. *Am. Zool.* **18**, 81–93.

PHILLIPS, H. M. & STEINBERG, M. S. (1978). Embryonic tissues as elastoviscous liquids. I. Rapid and slow shape changes in centrifugated cell aggregates. *J. Cell. Sci.* **30**, 1–20.

PRESS, W. H., FLANNERY, B. P., TEUKOLSKY, S. A. & VETTERLING, W. T. (1986). *Numerical Recipes, The Art of Scientific Computing*. pp. 274–334. Cambridge: Cambridge University Press.

PRUSINKIEWICZ, P. & LINDENMAYER, A. (1990). *The Algorithmic Beauty of Plants*. New York: Springer-Verlag.
PURCELL, E. (1977). Life at low Reynolds number. *Am. J. Pathol.* **45**, 3–11.
ROGERS, G. & GOEL, N. (1978). Computer simulation of cell movements: cell-sorting, cellular migration through a mass of cells and contact inhibition. *J. theor. Biol.* **71**, 141–166.
ROGERS, T. & SAMPSON, J. (1977). Computer simulations of surface tensions in cellular aggregates. *Inter. J. Bio. med. Comp.* **8**, 45–68.
SCHULZE, G. E. W. & WILBERT, H.-P. (1989). Chord intercepts in a two-dimensional cell growth model. Parts I, II. *J. Mater. Sci.* **24**, 3101–3106; 3107–3112.
SMITH, C. S. (1954). The shape of things. *Sci. Am.* **190**, 58–64.
STEINBERG, M. S. (1963). Reconstruction of tissues by dissociated cells. *Science* **141**, 401–408.
STEINBERG, M. S. (1970). Does differential adhesion govern self-assembly processes in histogenesis? Equilibrium configurations and the emergence of a hierarchy among populations of embryonic cells. *J. exp. Zool.* **173**, 395–434.
STEINBERG, M. S. (1975). Adhesion guided multicellular assembly: a commentary upon the postulates, real and imagined, of the differential adhesion hypothesis, with special attention to computer simulations of cell-sorting. *J. theor. Biol.* **55**, 431–443.
STEINBERG, M. S. & GARROD, D. R. (1975). Observations on the sorting-out of embryonic cells in monolayer culture. *J. Cell Sci.* **18**, 385–403.
SULSKY, D., CHILDRESS, S. & PERCUS, J. K. (1984). A model of cell sorting. *J. theor. Biol.* **106**, 275–301.
TAKEICHI, M. (1991). Cadherin cell adhesion receptors as a morphogenetic regulator. *Science* **251**, 1451–1455.
TANEMURA, M., OGAWA, T. & OGITA, T. (1983). A new algorithm for three-dimensional Voronoi tessellation. *J. Comput. Phys.* **51**, 191–207.
TOWNES, P. L. & HOLTFRETER, J. (1955). Directed movements and selective adhesion of embryonic amphibian cells. *J. exp. Zool.* **128**, 53–120.
TRINKAUS, J. P. (1984). Mechanisms of *Fundulus* epiboly—a current view. *Am. Zool.* **24**, 673–688.
TRINKAUS, J. P., TRINKAUS, M. & FINK, R. D. (1992). On the convergent cell movements of gastrulation in *Fundulus*. *J. exp. Zool.* **261**, 40–61.
WEAIRE, D. & RIVIER, N. (1984). Soap, cells and statistics—random patterns in two dimensions. *Contemp. Phys.* **25**, 59–99.
WELIKY, M., MINSUK, S., KELLER, R. & OSTER, G. (1991). The mechanical basis of cell rearrangement. II. Notochord morphogenesis in *Xenopus laevis*: simulation of cell behavior underlying tissue convergence and extension. *Development* **113**, 1231–1244.
WELIKY, M. & OSTER, G. (1990). The mechanical basis of cell rearrangement. I. Epithelial morphogenesis during *Fundulus* epiboly. *Development* **109**, 373–386.

APPENDIX A

Free Dirichlet Tiling

The positions $\vec{r}_i$ of N cell centers C_i suffice to label a pattern. We follow a standard Dirichlet tiling algorithm (Tanemura *et al.*, 1983). To determine the neighbors of C_1, we first calculate the distances to other centers, $r_{1j} = |\vec{r}_j - \vec{r}_1|$, and keep only the centers with $r_{1j} < 2R$, labeled $C_2 \ldots C_5$ in Fig. 16. Among them we look for C_2 such that $r_{12} = \min_k(r_{1k})$; cells 1 and 2 are necessarily in contact. We then look for the center C_3 such that the circle including C_1, C_2 and C_3 is the smallest; this circle is centered on the point P_{123} where the mediatrices meet, i.e. the triple contact between the three cells. We then determine progressively the set of successive neighbors.

We calculate all the geometrical quantities of a two-dimensional pattern by decomposing them over pairs and triplets of neighbors. For instance, the contact length between cells 1 and 2 is the sum of the lengths $Q_{12}.P_{123}$ and $Q_{12}.M_{12}$. The length $Q_{12}.P_{123}$, as the other elementary quantities of the triangle $C_1.C_2.C_3$, is a symmetric function of its side lengths r_{12}, r_{23}, r_{31} alone, and is independent from the positions of other centers (Tanemura *et al.*, 1983). Similarly, r_{12} and R alone

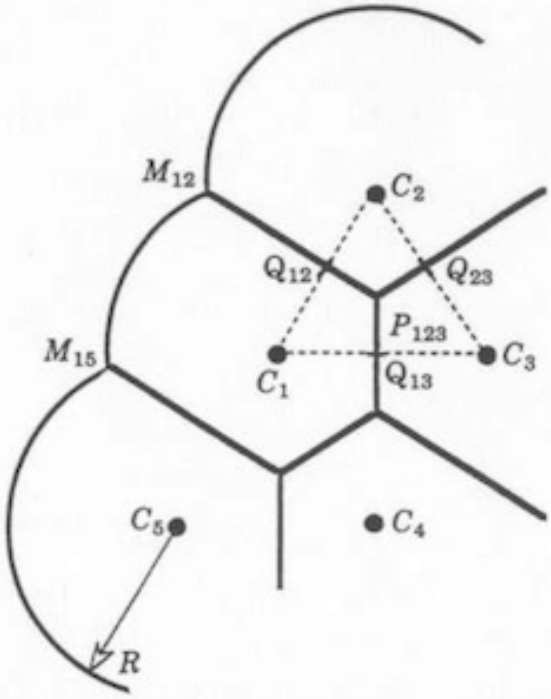

FIG. 16. Free Dirichlet domains in two dimensions. C_i is the Dirichlet center of domain i. The membrane between domains i and j is the mediatrix of C_i and C_j and Q_{ij} is their middle. M_{ij} is at a distance R from both C_i and C_j, and P_{ijk} is equidistant from C_i, C_j and C_k.

determine the length $Q_{12} \cdot M_{12}$, and r_{12}, r_{25}, r_{51} and R determine the free arc $M_{12} \cdot M_{15}$. We then decompose the total surface energy E_{adh} over each membrane portion. In three dimensions the surface energy of free Dirichlet domains is also a simple function of relative distances between pair, triplets and quadruplets of neighbors.

We then calculate the energy gradient with respect to the relative distances. The center C_j exerts upon C_i a force $\vec{F}_{\text{adh}}(j \to i) = -\partial E_{\text{adh}}/\partial \vec{r}_{ji}$. Since $r_{ji} \cdot \mathrm{d}r_{ji} = \vec{r}_{ji} \cdot \mathrm{d}\vec{r}_{ji}$, this force is equal to:

$$\vec{F}_{\text{adh}}(j \to i) = -\frac{\partial E_{\text{adh}}}{\partial r_{ji}} \frac{\vec{r}_{ji}}{r_{ji}} = \frac{\partial E_{\text{adh}}}{\partial r_{ij}} \frac{\vec{r}_{ij}}{r_{ij}}, \tag{A.1}$$

and is thus parallel to $\vec{r}_{ij}$ (more generally, the gradient of a function of $|\vec{r}|$ is always parallel to $\vec{r}$). If C_k is a neighbor sharing a vertex with C_j and C_i, this force is a function of r_{ij}, r_{ik} and r_{jk}, symmetric in r_{ik} and r_{jk}. Sulsky *et al.* (1984) derived a similar formalism for standard Dirichlet domains. We take into account both free and bound membranes.

APPENDIX B

Finite Cell Size

Simulations of biological cells include a finite length scale stabilizing the cell against coarsening. This constraint is usually implicit: finite or periodic boundary conditions fix the average volume allocated to each cell. We explicitly introduce in

the total energy E_{total} a term E_{stab} which maintains the cell size near R. As we already compute the perimeter length L for the adhesion term E_{adh}, we use a perimeter elasticity, $E_{stab} = 1/2\kappa(L-L_o)^2$. Since E_{stab} involves simultaneously all the neighbors of one domain, the effective center–center interaction is non-local. We calculate analytically the total potential energy $E_{total} = E_{adh} + E_{stab}$ as a function of the r_{ij}, but we cannot separate it into single vertex contributions.

We can make other choices to describe, for instance, bulk compressible cells, vacuolized cells, or a 2D section of 3D cells with variable height. As our domains are convex, these choices are roughly equivalent and do not affect the evolution of simulated patterns. However, a pressure term alone is not sufficient to prevent the instability of the cell size. We can also describe incompressible cells if we use the dynamic equations defined by Sulsky *et al.* (1984). Real cells have a more complex constitutive relation between area, volume and applied forces.

If the target perimeter L_o is greater than the perimeter $L_f = 2\pi R$ of 2D free cells, the cells tend to become free, they disperse and gaps appear. If L_o is much smaller than L_f, the cells tend to decrease their perimeter and shrink slightly. We can extend the model by setting a different target perimeter for dark and light cells [Fig. 3(a)] or letting R and L_o vary [Fig. 3(b)]. We set $L_o/L_f = 0{\cdot}8$ in all the 2D simulations shown.

κ is a Lagrange multiplier associated with the perimeter conservation constraint. If $\kappa \cdot L_f$ is much smaller than the differences in surface energies (or surface tensions), the size constraint is ineffective and cells grow (if surface energies are negative) or shrink (if surface energies are positive). If $\kappa \cdot L_f$ is much greater than the surface tensions, the pattern freezes. We fix $\kappa \cdot L_f = 5E_o$ in Fig. 13, $\kappa \cdot L_f = 3E_o$ in Figs 2, 10, 11, 14, 15, and $\kappa \cdot L_f = E_o$ in Figs 5–9, 12, 15, i.e. roughly half the maximal surface tension acting on the cells. We find that in this regime the perimeter constraint does not affect the evolution of the shape or the position relaxation. Our simulations are barely sensitive to the value of L_o.

APPENDIX C

Time Evolution

Equation (6) defines the forces $\vec{F}_i$ for a given configuration. Each iteration of the simulation simultaneously moves each center, according to eqn (7), by a displacement vector $\Delta\vec{r}_i = \vec{F}_i \Delta t/\mu_c$. A new configuration is then reached and another time step begins. This simultaneous updating is close to actual cell movements, but using a discrete time step raises some numerical difficulties.

We usually choose a time increment small compared to the time scale τ_o, for example, a hundredth. To avoid any divergence of the displacement when a cell passes near a singularity of the energy landscape, we require that $|\Delta\vec{r}_i|$ is never greater than a maximum, Δ_{max}. In practice, we compute the greatest force which acts on a cell, $F_{max} = \max_{(i)}|\vec{F}_i|$. The time increment is then:

$$\Delta t = \min\left[\frac{\Delta_{max}\mu_c}{F_{max}}, 0{\cdot}01\tau_o\right]. \qquad \text{(C.1)}$$

The elapsed time t increments by Δt at each step and this integrated time is displayed.

We choose a small value $\Delta_{max} = 0{\cdot}1R$ for the simulations of dissociating heterogeneous systems (Figs 9 and 15). We checked that the patterns and the total integrated time are the same if we chose a smaller Δ_{max}. Homogeneous patterns have a smoother energy landscape and tolerate quicker computations, so we use $\Delta_{max} = 0{\cdot}2R$ in Figs 5–7.

Large relative movements of the cells are slower processes. Some regions of the energy landscape are very flat. For instance, a cell attracted in two different directions at the same time feels a weak resultant force. To break the symmetry of such an unstable energy extremum, the cell needs to move a finite length and intercalate between its neighbors. It takes an infinite time if we constrain too severely the maximum displacement. Let this cell, subject to a weak resultant force, make a small movement. Then, during the same time step, another cell, in a region where the energy landscape has a steep slope, may move a long distance. Thus, at each step we allow at least one cell to move by setting $\Delta_{max} = 0{\cdot}5R$, in Figs 8 and 10–14. The problem is that a few cells may oscillate around a singular energy minimum (for example, a neighbor exchange), instead of relaxing. Allowing such a high discrete displacement does not introduce any randomness; it only favors the proper movement of a few cells. This accommodation is necessary to escape from the saddle points of the energy landscape but does not artificially breach potential energy barriers, so metastable states are preserved [Figs 13(c′) and (14)].

The initial calculation of free Dirichlet domains is time-consuming (Appendix A). Due to the finite size of the domains, each center has neither neighbors further than $2R$, nor very close neighbors. Most domains have five to seven sides, fewer for cells with a free surface. The maximum number of neighbors n_{max} is then always less than ten for the initial pattern, and even less after equilibration (n_{max} is slightly higher in three dimensions). Thus, storing a whole pattern of N cells only requires DN parameters for the center positions, where $D = 2$ in our simulations, and a symmetric $N \cdot (n_{max})^2$ array of relative distances between a center and its neighbors.

As we fix Δ_{max} we know that we need not renew the total computation of Dirichlet domains at each step, as only a cell within a distance R/Δ_{max} can become a new neighbor. Thus, the computation time, like the storage capacity, is of the order $N \cdot (n_{max})^2$ (Tanemura *et al.*, 1983).

More sophisticated algorithms of gradient descent could be used (Press *et al.*, 1986) but would not solve the double difficulty that neighbor exchange creates singularities (i.e. strong oscillations) and that at the same time other cells which are subject to much weaker forces are more essential to the simulation (see e.g. Sulsky *et al.*, 1984). Our choice was guided by the efficiency of computing Dirichlet domains, since it requires only one computation per time-step. The program is available upon request.

APPENDIX D

Viscosity of a Cellular System

Viscosity appears in the literature in two mutually exclusive forms, cellular and fluid. Using the Navier–Stokes equation treats the cell collection as a continuous

fluid (Gordon *et al.*, 1972; Phillips & Steinberg, 1978). The viscous force per unit volume is much bigger than the inertial term (Purcell, 1977):

$$\mu_f \Delta \vec{v} \gg \frac{D(\rho \vec{v})}{Dt}, \tag{D.1}$$

as is easily shown by considering the dimensionless Reynolds number $Re = cR\rho/\mu_f$. Here, $c = |\vec{v}|$ stands for velocity, R for typical cell size, ρ for density and μ_f for fluid viscosity. For an estimate, we can at least assume that μ_f is much greater than the viscosity of water:

$$\mu_f > 10^{-2} \text{ poise}, \tag{D.2}$$

or equivalently that:

$$\nu_f = \mu_f/\rho > 10^{-2} \text{ cm}^2 \text{ sec}^{-1}. \tag{D.3}$$

One cell radius R and speed c can be as large as 10^{-3} cm and 10^{-4} cm sec^{-1} for hydra cell aggregates (Sato, M. & Graner, F., unpublished data), but c is much smaller in intact tissues such as natural embryos; Odell *et al.* (1981) use 10^{-2} μm sec^{-1}. Certainly, Re is less than

$$10^{-3} \text{ cm} \times 10^{-4} \text{ cm sec}^{-1}/10^{-2} \text{ cm}^2 \text{ sec}^{-1} \sim 10^{-5}, \tag{D.4}$$

and might be 10^5 times smaller if $\mu_f \approx 10^3$ poise, as Evans (1983) estimates for white blood cell cytoplasm, or 10^8–10^{10} times smaller if μ_f lies in the range $0{\cdot}4 \times 10^6$ to $0{\cdot}7 \times 10^8$ poise, as Gordon *et al.* (1972) estimate for embryonic cells aggregates.

On the other hand, in a discrete cellular formalism the Newtonian equations of motion for a single cell yields:

$$m \frac{d\vec{v}}{dt} = -\mu_c \vec{v} + \sum \vec{F}. \tag{D.5}$$

The coefficient μ_c stands for a "cellular viscosity" (Odell *et al.*, 1981; Weliky & Oster, 1990; Weliky *et al.*, 1991); it could even be anisotropic if we separately defined shear and compression values. It also dominates the inertial term and the equation of motion becomes:

$$\vec{v} = \frac{1}{\mu_c} [\sum \vec{F}], \tag{D.6}$$

where μ_c^{-1} is the cell mobility. Confusion can arise from the notation μ and subscripts are needed because μ_c is not a true viscosity, having the dimension of poise · cm, or g · sec^{-1}.

The fluid description has the merit of linking the dissipation to spatial variations of velocity, instead of absolute velocity, while the cellular one emphasizes the discontinuous, independent behavior of different objects. The difference between absolute and relative velocities is not essential as long as each cell moves more than the average motion of its neighbors, i.e. there is no global drift. These two aspects have been formalized by Sulsky *et al.* (1984) using incompressible Dirichlet domains. In general, intuitive correspondence between both descriptions can be realized by thinking of a single cell moving within an immobile cell mass. The Laplacian of the velocity field, $\Delta \vec{v}$, is of the order $\vec{v}/R^2$ and the force per unit volume $-\mu_f \Delta \vec{v}$ is exerted

on a volume roughly of the order R^3, so that compatibility of both descriptions is ensured only if:

$$-\mu_f \frac{\vec{v}}{R^2} R^3 = -\mu_c \vec{v}, \tag{D.7}$$

or

$$\mu_c = \mu_f R. \tag{D.8}$$

With R of order 10^{-3} cm and the value of μ_f estimated by Gordon *et al.* (1972), μ_c lies within the range 10^3 to 10^5 poise·cm (or $g \cdot sec^{-1}$).